Driving micro-scale object by a dc electric field

Tomo KURIMURA

Abstract

In this thesis, we report on bifurcation analysis of a water droplet oscillating in an oil phase under a dc electric field. From this analysis, we expected that the addition of noise would induce the coherence oscillation of the oscillating water droplet. We also demonstrated that the addition of noise to a dc bias voltage induced this coherent motion of the droplet in our experiment. We also employed oil flow containing plastic beads instead of a water droplet in an oil phase under a dc voltage. We could observe rotation of the droplets and assumed it to be caused by the oil flow.

On the nano- and micro scales, the viscosity is much larger than inertia. Furthermore, we cannot ignore thermal fluctuations on such scales. Under these conditions, it is difficult to drive a micro- or nano-sized object made by a conventional method typically employed on macro scale. One solution is to apply the relevant phenomena on the microscale. In the present study, We attempted to use a water droplet oscillating in an oil phase under a dc electric field as a novel mechanism for driving a micro- or nano-sized object. To accomplish this, we investigated the oscillating mechanism in this thesis.

In Chapter 3, we report on the bifurcation analysis of a water droplet oscillating in an oil phase under a dc electric field. In our experiment, we changed both the distance and the voltage between the electrodes. This oscillation phenomenon of a water droplet in an oil phase under a dc electric field is well known since the 1990s. However, the threshold voltage has thus far not been determined, and its dependence on the scale of the system has not been evaluated. To our best of our knowledge, the present study is the first attempt to reveal the scale dependence of the oscillation phenomenon. We also made a numerical model of the droplet motion in the oscillation phenomena, on the basis of which we expected the droplet oscillation to be the limit cycle oscillation. We also expected that the addition of noise stabilize the oscillation near the threshold voltage. In Chapter 4, we evaluated this expectation. We added Gaussian white noise to a dc bias voltage. Although the voltage between the electrodes was slightly smaller than the threshold voltage, the additional noise enhanced the oscillation of the water droplet in the oil phase. We examined the dependence of the droplet motion on the magnitude of noise and found a suitable magnitude of noise exists at which oscillation of the droplet occurs. We think that this droplet oscillation is a kind of coherence resonance. The nature of the oscillation as the limit cycle is crucial for driving a micro- or nano-sized object, since the limit cycle is stable against disturbances. Droplet oscillation also generates coherence resonance, which is a desirable characteristic for the micromachines functioning in noisy environments to account for instabilities such as thermal fluctuation and so on.

In this study, we found that a water droplet oscillating in an oil phase under dc voltage has some beneficial characteristics. Nevertheless, the water droplet is unsuitable in some scenarios. Water droplets suffer from the disadvantage of easily breaking up and coalescing under an electric field. To overcome these disadvantages, we used plastic beads instead of a water droplet in the present study, as described in Chapter 5. As a result, we observed that they rotated between the electrodes. Since plastic beads are not conductive, we did not consider them to be charged. We expected this rotation to be caused by electrohydrodynamic (EHD) flow. We calculated the EHD flow numerically and obtained a vortex similar to that of the rotating beads. As a result, we confirmed that EHD flow caused the rotation of the beads. EHD flow is commonly

used to drive a micro-pump. However, it has not been used as a power source for driving a microsized object. In the present study, we found that EHD flow could be used to drive a microsized object. Although generation of rotational motion on the microscale is difficult because of large friction, we were able to generate a rotational motion under a dc electric field.

In summary, we examined the scale dependence of the oscillation of a water droplet in an oil phase and found the oscillation to be a limit cycle and to have a characteristic of coherence resonance. We also confirmed that EHD flow could rotate a microsized object under a dc electric field and established a novel mechanism for driving a microsized object. We anticipate this mechanism to be applicable to a micromachines in the future.

List of papers

This thesis is based on the following original papers. The chapters which include the contents of the papers are indicated:

Published papers

[1] Tomo Kurimura, Masahiro Takinoue, Kenichi Yoshikawa and Masatoshi Ichikawa "Back-and-forth micromotion of aqueous droplets in a dc electric field", *Physical Review E* **88** 042918(2013): Part 3 [1].

Papers under submission

[2] Tomo Kurimura and Masatoshi Ichikawa
"Noise-supported actuator: Coherent resonance in the oscillations of a micrometer-sized object under a dc-voltage", (2015): Part 4.

Reference paper

[3] Ryota Yamamoto, Daigo Yamamoto, Akihisa Shioi, Shuji Fujii, Tomo Kurimura and Kenichi Yoshikawa
"Arrangement and Periodic Motion of Microparticles in an Oil Phase under a DC Electric Field" *Journal of the Society of Powder Technology*, **51**(12) 823-827 (2014). [2]

Contents

Chapter 1

General Introduction

1.1 Perspective

At the micrometer scale, information is sticky and noisy (Fig. 1.1). Furthermore, at this scale, viscosity is dominant over inertia. Autonomous regular motions in a microfluidic system, *i.e.*, with Reynolds number; Re $\ll$ 1, generally require continuous supply of energy, since the viscosity or dissipation term becomes much more significant than the inertia term for motion in such a system [3]. Moreover, thermal fluctuation becomes significant in the motions of micro- to nanosized objects.

Progress in the field of microfabrication has facilitated development of microscale technologies such as the microelectromechanical system (MEMS) technology, micro-total analysis system (μTAS) technology [4], and 3D laser fabrication [5, 6]. However, owing to the abovementioned problems, in the fablication of a small object mimicking a conventional engine, it is challenging to reproduce the desired motion as can be done on the macroscale. Therefore, there is a need to establish an innovative approach to drive nano- and micromachines.

One way to overcome these problems is to explore or employ the mechanism of biological motor proteins, which already exist in microorganisms (Fig. 1.2). Biological motor proteins are usually present between the membranes that devide the inside of the cell from its surroundings. They use the potential difference between the outer and inner boundaries of the cell for movement. Studies on various biological motile systems such as flagella, cilia, and other locomotive systems have been conducted to clarify the mechanisms that underlie their energy transformation strategy [7–10]. Although complete construction of an artificial motor protein has not yet been realized, some research groups have utilized microorganisms as a power source for micromachine [11, 12]. Nevertheless, the features of the mechanism of the biological motor proteins are capable of being utilized in generating forces of the surrounding noisy environment.

In nonlinear and nonequilibrium physics, limit cycle oscillation is considered a suitable system for a noisy environment.A detailed introduction of limit cycle oscillation is provided in Chapter 2. In limit cycle oscillation, only one trajectory is independent of the initial condition, thereby indicating the robustness of this limit cycle oscillation. If we can find a limit cycle oscillator on the microscale, it would be highly useful in realizing an efficient micromachine.

Therefore, this thesis focused on the oscillation of a droplet/particle in an oil phase under a dc electric potential. Many groups have studied this kind of system from scales ranging from the sub-milimeter scale to centimeter scale. However, the threshold voltage for this system has not yet been determined, and its dependence on the scale of the system has not been explored. In this study, first, we reduced the scale of this system to the microscale. This system converts electric energy to kinetic energy, which is the

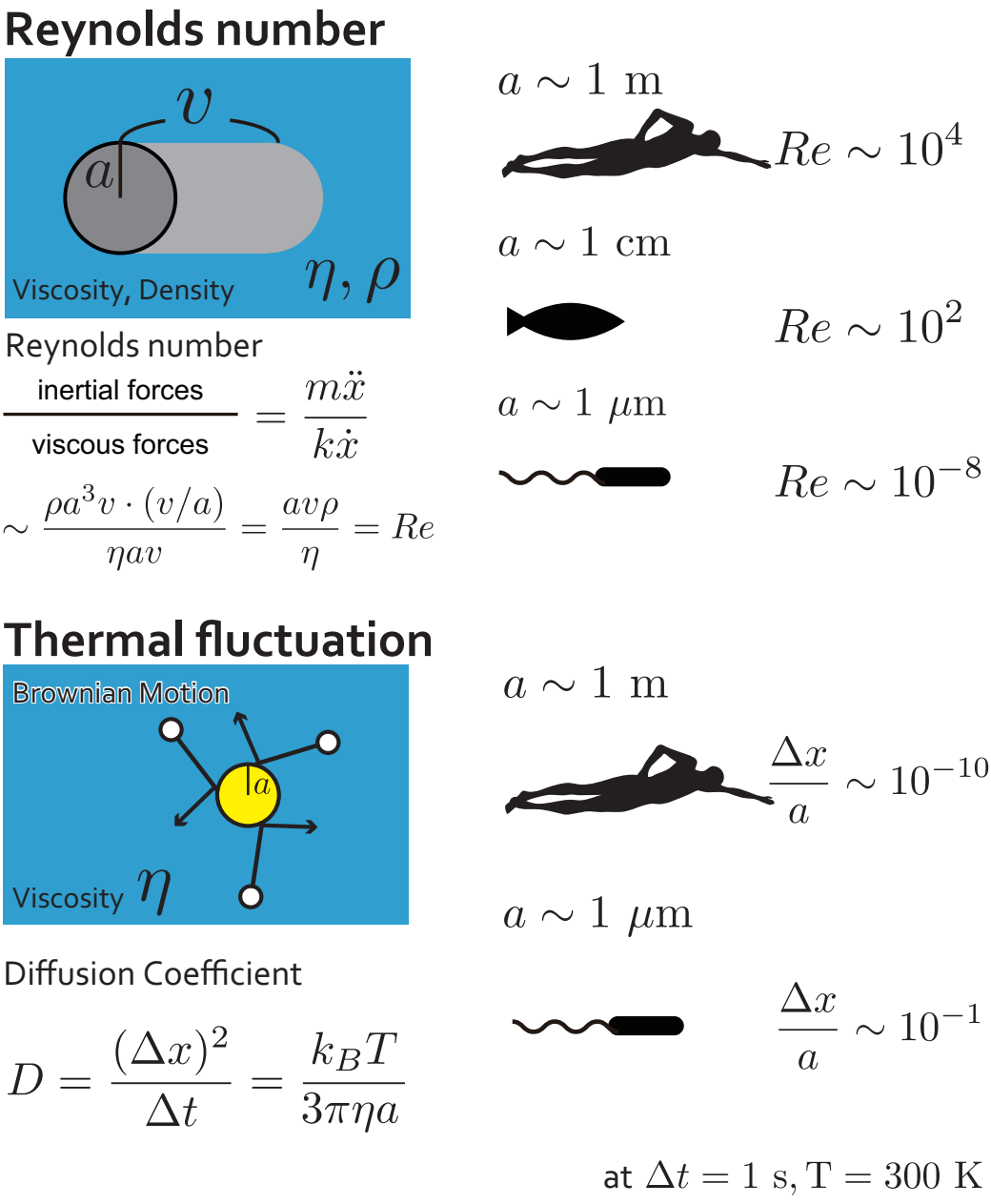

FIGURE 1.1: Viscosity and thermal fluctuation are not of concern during swimming or running motion. However, when an object is microsized, viscosity is dominant over inertia. In this case, thermal fluctuations are also comparable to the size of the object.

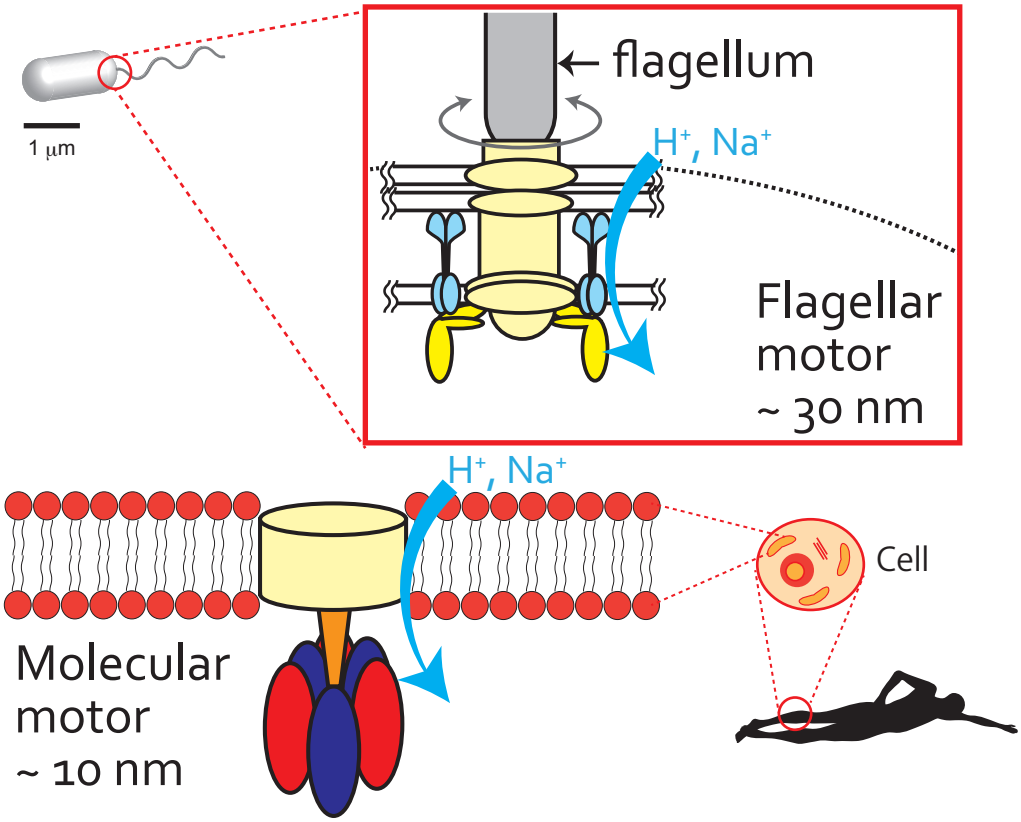

FIGURE 1.2: In a situation where the viscosity and thermal fluctuation are dominant, protein motors in microorganisms and minute organs in cells can generate the desired force efficiently.

same principle as that of biological motor proteins. Investigation of the behavior of a microsized droplet oscillating under a dc voltage is connected to gaining an understanding of the motor protein. The oscillation of the droplet is caused by the balance of energy pouring into the system and its dispersion. In this study, we demonstrate that the oscillation is a limit cycle oscillation. We also demonstrate that his system is robust against fluctuations. We investigate some aspects pertaining to this oscillation to enable realization of a micromachine by means of a proposed novel mechanism.

1.2 Outline of thesis

In Chapter 2, two important topics for discussion pertaining to this thesis are introduced: (1) Limit cycle and coherence resonance and (2) droplet oscillation between the electrodes under a dc voltage in an oil phase. WeThis chapter also introduces a few topics related to a microsized object in a dielectric liquid under an electric voltage.

In Chapter 3, back-and-forth micromotion under a dc electric field is described. We reduced the scale of the droplet oscillation system to the microscale and investigated the bifurcation of the droplet motion. It is important to establish the bifurcation point between the oscillatory state and the stationary state for driving the microsized droplet. In this study, we found that this oscillation is a limit cycle oscillation. This feature of the microsized droplet oscillation system is suitable for its application to the micromachines. The contents of this chapter have been published in paper [1] listed at the beginning of papers.

In Chapter 4, the coherence resonance occurring in the oscillatory motion of the microsized droplet is demonstrated. To examine the stability of the droplet oscillating under a dc electric field, we add noise to the oscillation system. As a result, the droplet is found to exhibit coherence resonance, which refers the oscillation induced by noise. If we apply this droplet oscillation system to a nano- or micromachine, we can not ignore the effects of thermal fluctuation. The characteristic of the droplet oscillation of being a kind of coherence resonance indicates that the oscillation can be stable even in such a noisy environment. The contents of this chapter have been published in paper [2] listed at the beginning of this thesis.

In Chapter 5, the effect of electrohydrodynamic (EHD) flow on the rotation motion of microparticles rotation in an oil phase is numerically simulated. When plastic beads are used instead of water droplets, they are observed to rotate between the electrodes, where this rotation is induced by the EHD flow. In this chapter, we first adopt EHD flow for analyzing the motion of a microsized object in an oil phase driven by an electric field. Unlike a water droplet, plastic beads are not charged. However, EHD flow can drive plastic beads under an electric field; this is the novel mechanism that we propose for driving a microsized object.

In Chapter 6, the contents of this thesis are summarized, and the future problems are presented.

Chapter 2

Background

2.1 Introduction

In this chapter, we introduce some fundamental topics aimed at understanding the contents of chapters from Chapter 3 onward. First, we are going to introduce a limit cycle as a nonlinear oscillator and the concept of coherence resonance related to a limit cycle. Then, we summarize studies on the oscillation of a droplet in an oil phase under a dc voltage. This is the primary topic of this thesis. We also explain a few topics pertaining to a microsized object in a dielectric liquid under an electric voltage.

2.2 Limit Cycle Oscillation and Coherence Resonance

2.2.1 Harmonic Oscillator

We typically learn about a Harmonic Oscillator during our high school and/or in the the first grade at university. This oscillator is fundamental and important to gaining an understanding of advanced phenomena First, the oscillator is in its equilibrium position. When some energy is added to it, it starts oscillating. This periodic motion is termed simple harmonic motion and is the reason why the oscillator is known as a harmonic oscillator. In simple harmonic motion, the restoring force is directly proportional to the displacement. One example of this motion is that of a spring. Let us consider a point mass with a spring (Fig. 2.1). When the point mass is at $x = 0$, it is in the

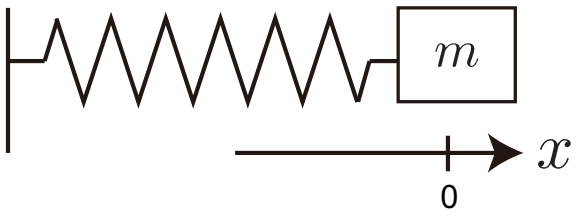

FIGURE 2.1: Point mass m and spring with the spring constant k. The displacement of the mass from the natural length of the spring is denoted as x.

equilibrium state. When displacement x is added to it, the equation of motion of the point of mass becomes

$$m\frac{d^2x}{dt^2} = -kx. \tag{2.1}$$

We can solve this equation analytically and obtain the sinusoidal motion, as shown in Fig. 2.2.

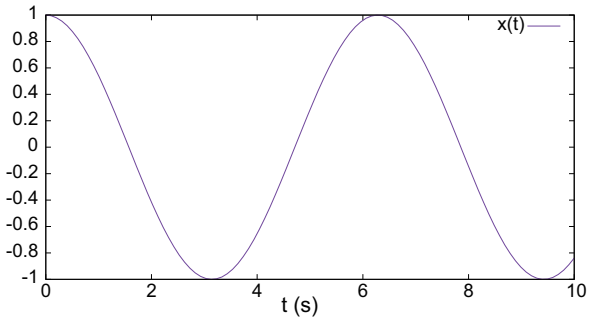

FIGURE 2.2: Analytical solution of Eq. 2.1.
The initial condition is $x(0) = 1$. For the sake of simplicity, we take $m = k = 1$.

This oscillation is ideal oscillation; it can not be observed in the world we live in. The reason for this is resistance. In the next section, we introduce a harmonic oscillator with resistance.

2.2.2 Harmonic Oscillator with Resistance

Resistance is the force that resists the motion. It can be of several kinds in the real world, such as friction and air resistance.

When resistance is proportional to the velocity, the equation of motion, *i. e.*, Eq.2.1 is modified as

$$m\frac{d^2x}{dt^2} + \gamma\frac{dx}{dt} = -kx. \tag{2.2}$$

This equation is not symmetric for time-inversion($t \to -t$). We solve this equation and acquire the oscillation with attenuation(Fig. 2.3).

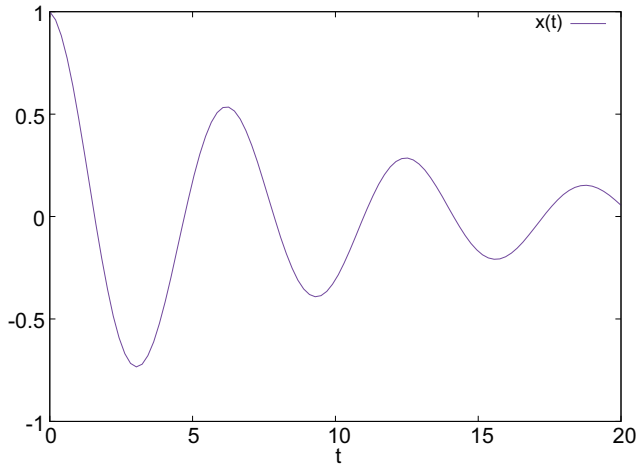

FIGURE 2.3: Analytical solution of Eq. 2.2.
The initial condition is $x(0) = 1$. We take $m = k = \gamma = 1$.

When $\gamma < 0$, the attenuation changes to amplification(Fig. 2.4).
,which means that energy is pouring into the system.

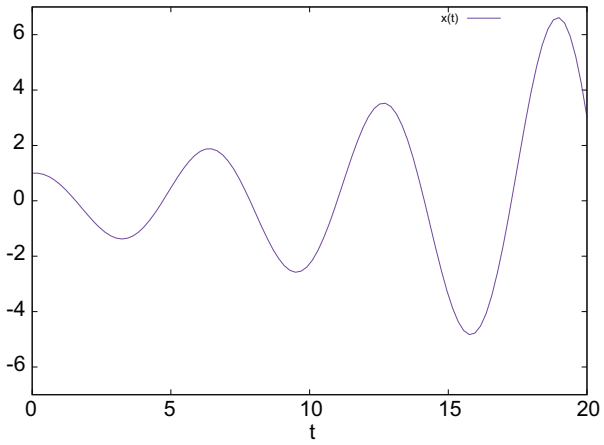

FIGURE 2.4: Analytical solution of Eq. 2.2 with $\gamma = -1$.
The initial condition is $x(0) = 1$. We take $m = k = 1$.

2.2.3 Limit Cycle Oscillation

As discussed in the previous section, when energy is poured the energy into a harmonic oscillator, it eventually approaches infinity. For example, when we sit on a swing, the action of pumping our leg during swinging pours energy into the swing. However, the swing does not approach infinity; this is because there is some resistance.

Let us add resistance to Eq. 2.2 with $\gamma < 0$ (Amplification). For the sake of simplicity, we set $m = k = 1$. For preparation, we write the equation in two-dimensional form as,

$$\frac{du}{dt} + \gamma u = -v \tag{2.3}$$

$$\frac{dv}{dt} = u. \tag{2.4}$$

In these equations, we denote the displacement as v and the velocity as u. Eqs. 2.3 and 2.4 are the same as Eq. 2.2. Then we add resistance to Eqs. 2.3 and 2.4. One solution is to add the force proportional to u^3 to Eq. 2.3.

$$\frac{du}{dt} + \gamma u + u^3 = -kv \tag{2.5}$$

$$\frac{dv}{dt} = u \tag{2.6}$$

Upon differentiating Eq. 2.5 with respect to t and substituting Eq. 2.6 into it, then we get

$$\frac{d^2u}{dt^2} + (\gamma u + 3u^2)\frac{du}{dt} = -u. \tag{2.7}$$

This equation represents the van der Pol oscillator. [1] This equation can be solved analytically in the limited condition. Here, we solve the equation numerically under different initial conditions; the obtained result is shown in Fig. 2.5. The obtained trajectories are the same under all these initial conditions. This is a feature of the limit cycle

[1] In 1926, van der Pol from Phillips (Company) discovered this equation. He first discovered this phenomenon in electric circuits employing vacuum tubes.[13]

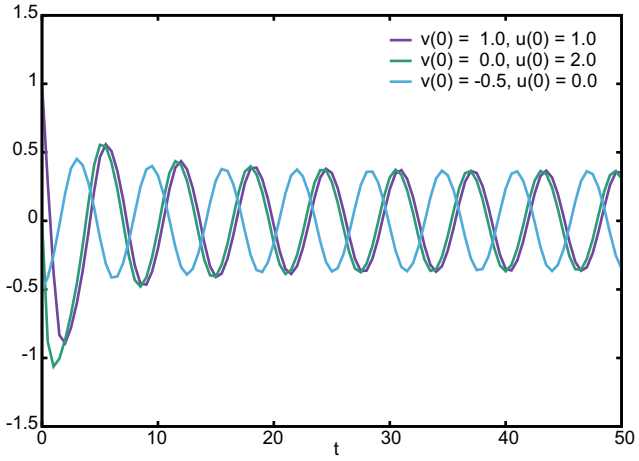

FIGURE 2.5: Numerical solution of Eqs. 2.5 and 2.6 with $\gamma = -0.1$. The initial conditions are indicated in the graph.

oscillation. In a harmonic oscillator, different initial conditions yield different trajectories. However, the trajectory of the limit cycle oscillation is independent of the initial condition.

Examples of the limit cycle are everywhere around us, *e. g.*, a firing nerve cell, a bowed violin string, flying aircraft and the Belousov-Zhabotionsky (BZ) reaction [14]. Of these examples, the BZ reaction, which is a chemical reaction that oscillates, has been studied extensively.

The color of a BZ solution changes synchronously over time. The oscillation of the color corresponds to the concentration of the chemical species is changed. The BZ solution does not oscillate when the combination of chemical species. However, when a silver wire is inserted in the solution, the color of the solution is observed to change at the point at which the wire touches the solution. What is the difference between these two phenomena? We explain this difference in the next section.

2.2.4 Bifurcation

To understand the phenomena introduced in the previous section, we first introduce a numerical model. We can write the equation that describe chemical reaction. However these equations are so complicated that understanding their behavior becomes difficult. A well-known numerical model for describing the BZ reaction is the Oregonator model. The equations of the Oregonator model (Tyson's version[15]) are as follows.

$$\epsilon \frac{du}{dt} = u - u^2 - fv\frac{u-q}{u+q} \tag{2.8}$$

$$\frac{dv}{dt} = u - v \tag{2.9}$$

To understand the behavior of these equations, we plot $du/dt = 0$ and $dv/dt = 0$ in a phase plane (Fig. 2.6). These lines are called nullclines, and the cross point is a fixed point[2]. When the point (u_0, v_0) is on the upper half of the $du/dt = 0$ line, $du/dt < 0$. When the point (u_0, v_0) is on the upper half of the $dv/dt = 0$ line, $dv/dt < 0$. Every

[2]We consider fixed point as the point where $(du/dt, dv/dt) = (0, 0)$. The system keeps stopping until it is driven by some external force.

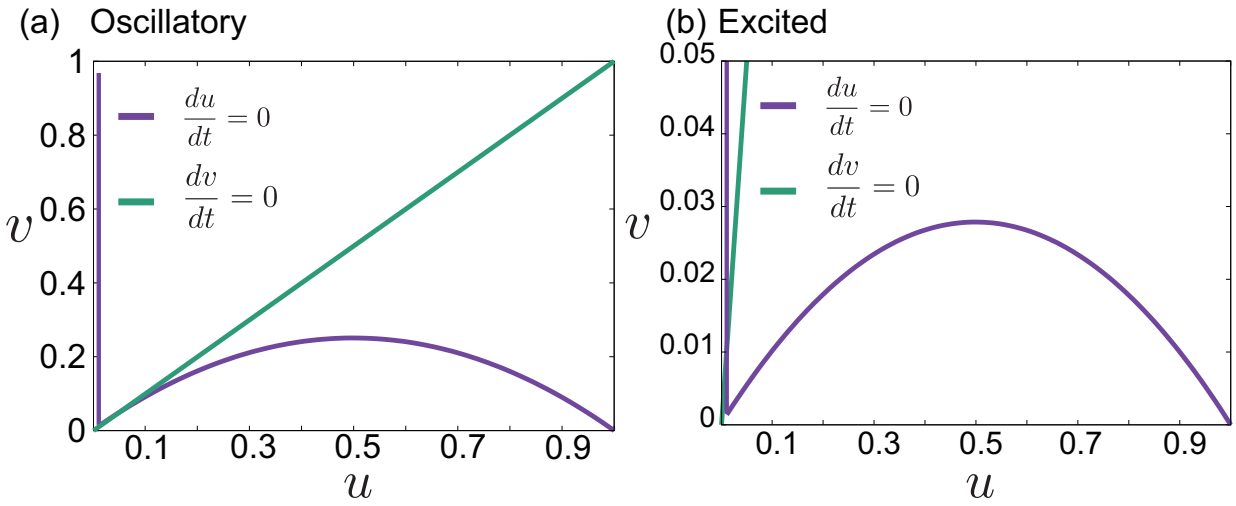

FIGURE 2.6: Nullclines of Eqs. 2.8 and 2.9. (a) Oscillatory state ($f = 1, q = 0.0008$) and (b) excited state ($f = 9, q = 0.0008$). The cross point is the fixed point.

point in the phase plane has $(du/dt, dv/dt)$ as the vector. Therefore, we can understand the behavior of the equations. The key factor for understanding this behavior is the position of the fixed point. We can investigate whether the fixed point is stable or unstable from the surrounding vectors. In Fig. 2.6, we can barely see where the fixed point is. To address this issue, we employ the equations whose behavior is the same as that of the Oregonator model:

$$\epsilon \frac{du}{dt} = u(1-u)(u-a) - v, \tag{2.10}$$

$$\frac{dv}{dt} = u - bv - I. \tag{2.11}$$

The nullclines are shown in Fig. 2.7 and they are similar to those of the Oregonator. When $a = b = I = \epsilon = 0$, these equations are the same as Eqs. 2.5 and 2.6.

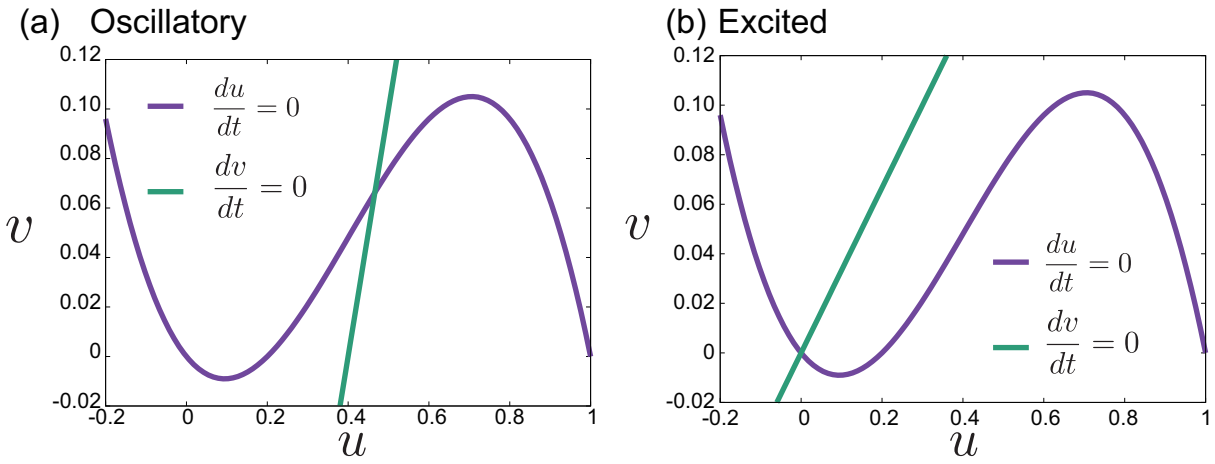

FIGURE 2.7: Nullclines of Eqs. 2.10 and 2.11. (a) Oscillatory state ($a = 0.2, I = 0.4, b = 1$) and (b) excited state ($a = 0.2, I = 0, b = 3$).

The $(du/dt, dv/dt)$ vectors are drawn as shown in Fig. 2.8. In Fig. 2.7(a), *i. e.*, the oscillatory state, we start the point P far from the stable point. In Eq. 2.10 du/dt is written with ϵ. This means that when the right-hand side of Eq. 2.10 is of the same order as that of Eq. 2.11 ,$du/dt \gg dv/dt$. Then, the system moves rapidly in the direction in which u becomes greater and stops when the point reaches the $du/dt = 0$ line. Now, the right-hand side of Eq. 2.10 is smaller than that of Eq. 2.11 . Then, when $du/dt \gg dv/dt$, the point move upward the $du/dt = 0$ line to the top. When the point reaches the top of the $du/dt = 0$ line, $du/dt \gg dv/dt$ again. Repeating this behavior, the system oscillates. This is known as a limit cycle. On the other hand, in the excited state (Fig. 2.7(b)), we start the point P far from the stable point. The point moves on the same track to the half way mark. However, a stable fixed exists point on the $du/dt = 0$ line. The point P eventually overlaps with the stable fixed point, and the system does not change. When we place the point P' near the fixed point, the point again moves back toward the fixed point again. If we add a large fluctuation to the point and let it move away from the fixed point, the point moves along the pseudo-track and comes back to the fixed point. This is the reason why this state is called the excited state. We can excite the system by adding large fluctuation.

By adjusting the relevant parameters, we can change the behavior of a nonlinear oscillator. This change in the behavior is called bifurcation, and it is one of the characteristics of a nonlinear system.

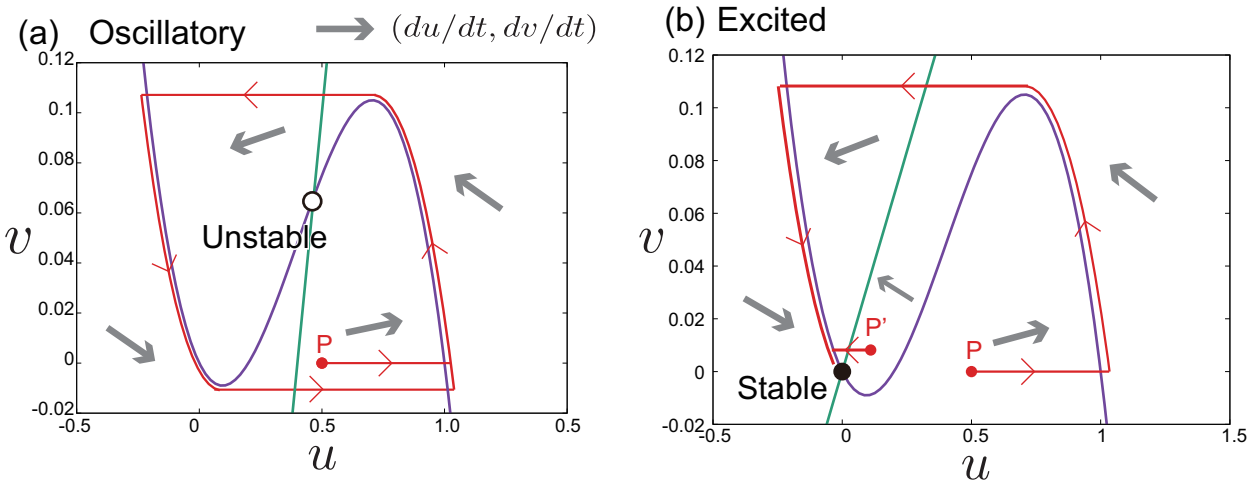

FIGURE 2.8: Nullclines with the vector $(du/dt, dv/dt)$. (a) In the oscillatory state, the system starts from the point P and shows the oscillation. (b) In the excited state, the system starts from the point P and eventually overlaps with the stable fixed point.

2.2.5 Coherence Resonance

As seen in the previous section, we can excite the system by adding a large fluctuation when it is in the excited state. Then what would happen upon adding a continuous fluctuation to a nonlinear system? In 1993, Gang found that addition of noisy force

could cause the system – which possesses a limit cycle – to oscillate similar to a limit cycle in which a parameter is smaller than its critical value [16]. Moreover, in 1997, Pikovsky and Kurths also found that a limit cycle similar to the oscillation in the Fitz Hugh-Nagumo (FHN) model can be generated in an excited state[17]. They termed this phenomenon as Coherence Resonance. Gang and Pikovsky demonstrated coherence resonance numerically; they revealed that there exists a suitable magnitude of noise at which a periodic motion can be generated. The schematic illustration of coherence resonance is shown in Fig. 2.9.

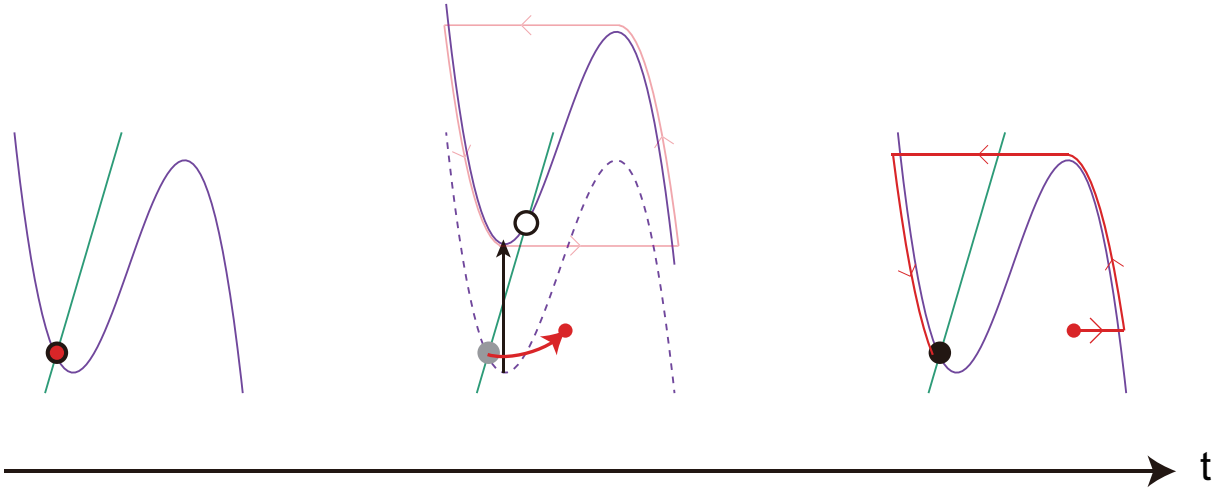

FIGURE 2.9: Schematic illustration of coherence resonance. First, the point remains at the fixed point. Next, noise perturbs the potential and the point escapes from the fixed point. Then the potential is restored and moves around the plane and back to the fixed point.

Here, we attempt to reproduce Gang and Pikovsky's numerical simulation. They used the FHN model with external noise,

$$\epsilon \frac{du}{dt} = u - \frac{u^3}{3} - v \tag{2.12}$$

$$\frac{dv}{dt} = u + a + D\xi(t). \tag{2.13}$$

where $\xi(t)$ is Gaussian noise with a zero mean and it has the relationship $< \xi(t)\xi(t') = \delta(t - t') >$. Further, D is the magnitude of noise. In this model, if $|a| < 1$, a limit cycle exists. On the other hand, if $|a| > 1$, only the attractor is a stable fixed point. We add noise to a system with $a = 1.05$, which is an excited state but near the bifurcation point. Figure 2.10 shows the results of the numerical simulation [3]. As can be seen from this figure, a suitable magnitude of external noise possibly exists at which an oscillation can be generated.

Coherence Resonance can also be reproduced experimentally. In this study, we employed the BZ reaction as an experimental example of a limit cycle. There are many kinds of BZ reactions. The BZ reaction is of several kinds. For example, one kind of

[3] We could not perform the numerical simulation with the same coefficients as those of Pikovsky and Kurths [17]. We instead used a Gaussian distribution having a zero mean and a variance is 1.0. We also consider $\epsilon = 1.0$. Though Pikovsky and Kurths [17] used the Euler method to solve the differential equations, we used the fourth-order Runge-Kutta method.

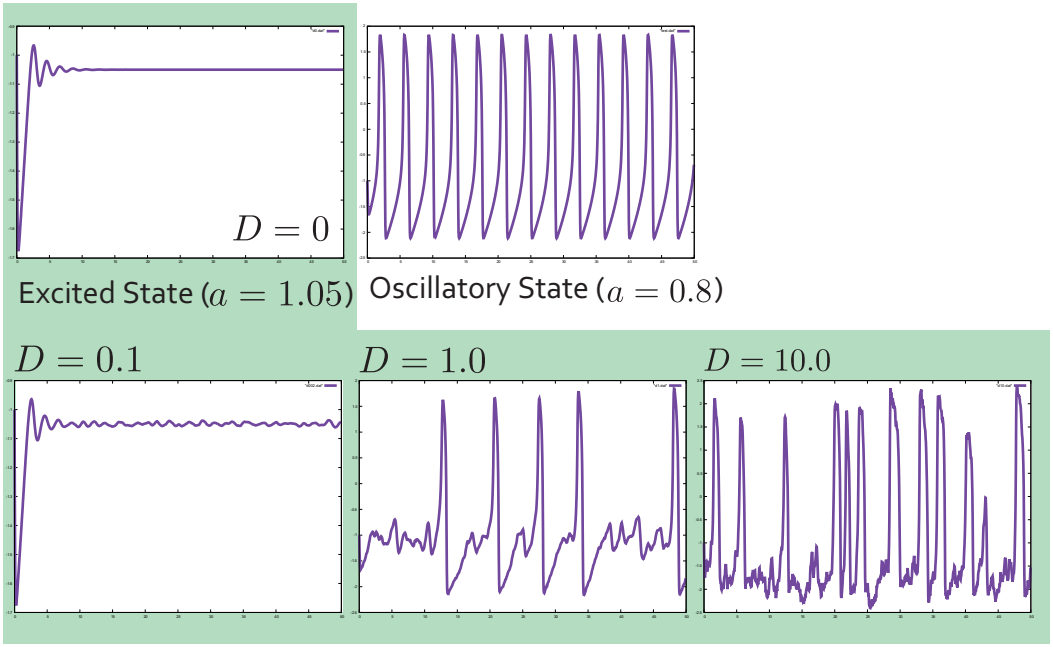

FIGURE 2.10: Results of numerical simulation. We added noise with magnitude D to the excited state in the FHN model. When $D = 0.1$, u vibrates around the fixed point. When $D = 1.0$, spikes similar to regular oscillation in the oscillatory state are observed. When D is increased to 10.0, the spikes seem to occur randomly.

BZ reaction is that which is activated by light, where the reaction can be controlled by controlling light. In this study, we adjusted a light-activated BZ reaction to the excited state and illuminated it with light with a random brightness level. As a result, we could observe pseudo oscillation.

2.2.6 Stochastic Resonance

Stochastic resonance is a phenomenon similar to coherence resonance. The difference between them is that stochastic resonance requires an external periodic force, whereas coherence resonance can generate a periodic motion just by the addition of noisy external force.

Next, we present an example of stochastic resonance. Let us consider about a dissipation system with the periodic external force.

$$\frac{\partial x}{\partial t} = -\frac{\partial V(x)}{\partial x} + \xi. \tag{2.14}$$

The dissipative force ξ is expressed as

$$< \xi(t_1)\xi(t_2) >= 2M\delta(t_1 - t_2). \tag{2.15}$$

The potential $V(x)$, which is the double-well potential, varies periodically, and it is written as

$$V(x) = -\frac{a}{2}x^2 + \frac{b}{4}x^4 - xh\cos(\Omega t). \tag{2.16}$$

Ω is the frequency of the external force. For the sake of simplicity, we take $a = b = 1$ and $h \ll 1$. The time dependence of $V(x)$ is shown in Fig. 2.11.

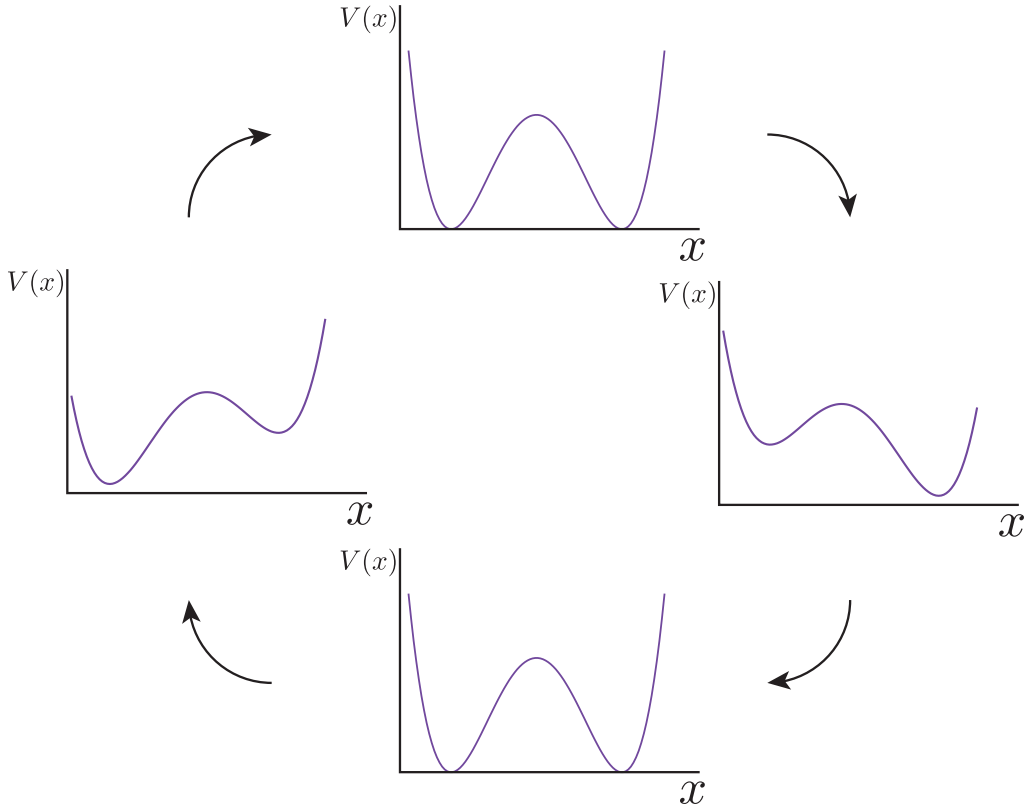

FIGURE 2.11: Schematic illustration of the time dependence of the potential $V(x)$(Eq. 2.16).

Let us consider the transition between each minimum state in the potential. We denote the probability of $x < 0$ as n_- and that of $x > 0$ as n_+; then, their time dependence of can be expressed as,

$$\frac{dn_\pm}{dt} = -W_\mp(t)n_\pm + W_\pm(t)n_\mp. \tag{2.17}$$

The normalized condition is

$$n_+ + n_- = 1. \tag{2.18}$$

W_+ is the transition rate from the left minimum to the right minimum and W_- is that one from the right minimum to the left minimum. If we determine $W_\pm$, we can obtain $n_\pm$.

When an external force is absent, we can linearize Eq. 2.14 around the equilibrium solution $x = \pm 1$. Then, we take $x = \pm 1 + \delta x$, and obtain $d\delta x/dt = -2\delta x$. Here, the relaxation rate is 2.

As the time development of the external force is adequately slower than this relaxation rate, $\Omega \ll 2$, the transition rate is determined by the shape of the potential at a particular time. If we consider the potential as expressed in Eq. 2.16, it becomes $V(x = 0) - V(x = \pm 1) = 1/4 \pm h\cos(\Omega t)$. We substitute this expression into Kramers'

formula [4] and obtain the probability of the transition rate as

$$W_{\pm} = k_0 \exp(\pm \frac{h}{M} \cos(\Omega t)), \tag{2.19}$$

$$k_0 = \frac{\sqrt{2}}{2\pi} \exp(-\frac{1}{4M}). \tag{2.20}$$

Upon expanding Eq. 2.19 using h, we get $W_{\pm}$

$$W_{\pm} = k_0[1 \pm \frac{h}{M} \cos(\Omega t) + O(h^2)]. \tag{2.21}$$

Upon substituting the normalized condition Eq. 2.18 in Eq. 2.17, we get

$$\frac{dn_{\pm}}{dt} = -(W_+ + W_-)n_{\pm} + W_{\pm}. \tag{2.22}$$

We can solve Eq. 2.22 and substitute Eq. 2.21 into the acquired solution for obtaining a long-time limit. Finally we get

$$n_{\pm}(t) = k_0 e^{-2k_0 t} \int_0^t da e^{2k_0 s}(1 \pm \frac{h}{M} \cos(\Omega s)). \tag{2.23}$$

Here we use the formulae

$$\int ds e^{as} \cos(bs) = \frac{1}{a^2 + b^2} e^(as)(a \cos(bs) + b \sin(bs)), \tag{2.24}$$

$$\cos(A - B) = \cos A \cos B + \sin A \sin B. \tag{2.25}$$

Then Eq. 2.23 becomes

$$n_{\pm}(t) = -\frac{1}{2} \pm \frac{h}{2M} \frac{2k_0}{\sqrt{4k_0^2 + \Omega}} \cos(\Omega t - \phi), \tag{2.26}$$

$$\tan \phi = \frac{\Omega}{2k_0}. \tag{2.27}$$

This $n_{\pm}(t)$ depends only on the time development of the external force.

We can calculate the time coefficient of x under a periodic external force and dissipation force by using Eq. 2.26 as

$$< x >= \int_{-\infty}^{\infty} dx \, x P(x, t). \tag{2.28}$$

The distribution function $P(x, t)$ of the two-state system in Eq. 2.16 is

$$P(x, t) = n_+(t)\delta(x - 1) + n_-(t)\delta(x + 1). \tag{2.29}$$

Then, we get

$$< x >= n_+ - n_-. \tag{2.30}$$

[4] This formula describes the transition rate from one state to another state in the potential. We can derive it by solving the Fokker-Prank equation to probability conservation and integrating it.

Substituting Eq. 2.23 into this equation, we get

$$< x >= A\cos(\Omega t - \phi) \tag{2.31}$$

$$A = \frac{h}{M}\frac{2k_0}{\sqrt{4k_0^2 + \Omega^2}}. \tag{2.32}$$

This is the first-order response of the system under a periodic external force and dissipation force.

We next investigate how the response amplitude A of the external force h depends the magnitude M of the dissipation force, when we fix this amplitude of the frequency of that Ω of the external force. Under the limit of $M \to 0$, according to Eqs. 2.20 and 2.32, A becomes

$$A \propto \frac{1}{M}e^{-1/4M}. \tag{2.33}$$

A is close to 0. However, if M increases, A decreases as $A \propto 1/M$. Thus, we except a certain value of M to give the largest value of A. A schematic illustration of this dependence is shown in Fig. 2.12.

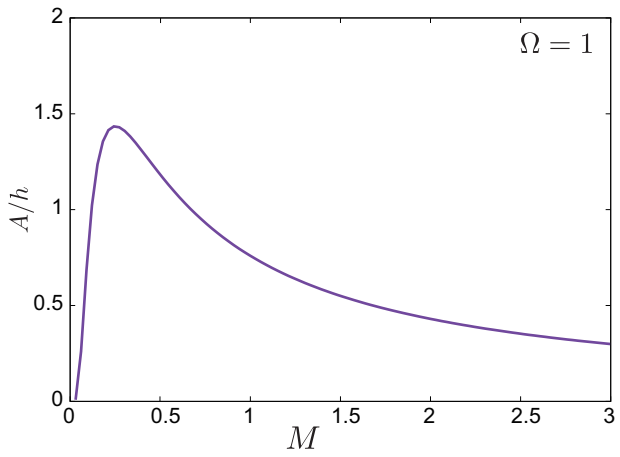

FIGURE 2.12: Dependence of amplitude A on magnitude M of noise with $\Omega = 1$. The curvature has a peak at $D \sim 0.5$.

As discussed in Sections2.2.6 and 2.2.5, we can derive a certain system we can drive by adding noise. These phenomena are effective mechanisms where we cannot ignore the noisy external force.

2.3 Review of Droplet Oscillation between Electrodes

In this section, we discuss previous studies on a conductive droplet oscillating between electrodes in a dielectric liquid. We also introduce some topics useful in understanding this oscillation mechanism.

2.3.1 Before Droplet Oscillation

It is known since the 1960s that a conductive droplet in the dielectric liquid can deform under application of an electric field. Taylor, a theoretician published a paper on the

Rayleigh-Taylor instability in 1950 and a paper on the deformation and flow inside and outside of a conductive droplet in a dielectric liquid under an electric field in 1966 [18]. His latter paper is based on the experiment by Allan and Mason in 1961 [19], who studied the effects of an electric field on the deformation of a droplet. In those days, researchers were interested in the deformation of a droplet under shear. Taylor also published a paper on the topic in 1934 [20]. Allan and Mason investigated electrical effect on a droplet.
Subsequently, some researchers studied the deformation of a droplet under an electric field in the flow. We believe that they observed a translational effect of the droplet under the electric field. However, no paper was published on the oscillation of a droplet between electrodes until 1990. For about 30 years before that, researchers studied heat and mass transfer by a droplet under an electric field. This transition of interest pertaining to a droplet in a dielectric liquid is depicted in Fig. 2.13.

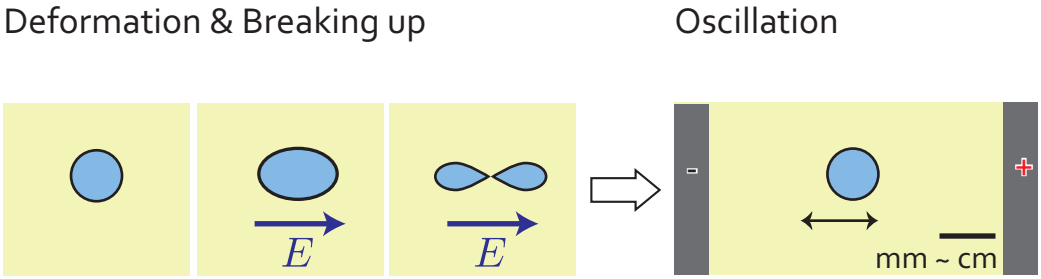

FIGURE 2.13: Schematic illustration of precious studies on a droplet oscillation. Before the 1990s, researchers were interested in the deformation, breaking up and coalescence of a conductive droplet in a dielectric liquid under an electric field. After the 1990s, the research interest shifted to oscillation of the conductive droplet.

2.3.2 Droplet Oscillation

The schematic illustration of these experiments we introduce next is shown in Fig. 2.14. In 1990, Mochizuki *et al.* first reported on the oscillation of a water droplet between electrodes under a dc voltage in an oil phase. They showed that the oscillation resulted in heat and mass transfer [21]. and also developed a numerical model, in which electric force and gravity were employed. In the model, the resistance was the viscosity of the rigid particle for the droplet. The model was found to well reproduce the results of an experiment, whose conditions were as follows; droplet diameter of about 5 mm; parallel-plate-type electrodes; distance of 25 mm between the electrodes; and dimethyl silicone oil (KF-96), n-heptane and FC-75 used as continuous phase.

In 2003, Eow *et al.* also observed that a water droplet exhibited translational motion between electrodes in n-heptane. They only evaluate the relationship between the velocity of the droplet and the force [22]. Eow *et al.* published the papers on this phenomenon in 2001 and 2002 [23, 24], they demonstrated that water could be eliminated from the oil phase by the application of an electric field. We believe that they discovered that droplet's translation phenomenon while attempting to determine a way to eliminate water from the oil phase.
On the other hand, in 2002, Khayari and Perez reported the oscillation of a metal particle between electrodes under a dc voltage [25]. Understanding the motion of a charged metal particle was crucial to understanding the phenomenon of dielectric relaxation,

which is of importance in the fields of academics and xerography. They also observed the period-doubling bifurcation of the oscillating metal particle experimentally [26]. The aim of their experiment was to measure the electric potential at the time when the particle was leaving one of the electrodes, and they did not investigate the oscillation itself. In their experiment, the electrodes were facing in the vertical direction. First, the particle remained on the bottom electrode because of gravity. Then once the voltage between the electrodes was increased, the particle acquired a charge and when the charged particle subjected an electric force, it left the electrode.

The oscillation of a droplet gained widespread research attention following the publication of Hase *et al.*'paper in 2006 [27]. By this time, the concepts of laser tweezer (2001) [28] and microfluidics (2005) has also become known. Furthermore, approaches for manipulating microsized objects were being established. In the study of Hase *et al.*, the size of the droplet was about 100 μm, and the distance between the electrodes was about 400 μm. Changing the dc voltage can enable, a change in the mode of the droplet motion to oscillation, bouncing, and adhesion to the electrode. Hase *et al.* also demonstrated a simple model, in which, they used an overdamped equation of motion owing to the small scale.

In the same year, Link *et al.* reviewed the application of an electric field in microfluidics. They introduced the coalescence of droplets and driving of a droplet in the desired direction by application of an electric field [29]. These phenomena were somewhat far from the oscillation of the droplet but they nevertheless related. In 2007, Kim *et al.* reported the motion and deformation of a droplet between electrodes [30]; they provided a precise formula of the force for including the deformation of a droplet. However, they did not show the time dependence of the formula. They first considered the effects of dielectrophoresis (we introduce this phenomenon in section 2.3.4). They also published a paper in 2008 [31], in which, they speculated the amount of charging of the droplet by observing its velocity. A figure of the droplet motion revealed that the droplet appeared to be driven at a constant velocity. The group of Kim *et al.* also studied droplet motion with the aim of applying it to microfluidics and using the droplet as a microreactor. In theirs studies, the scale of the distance between the electrodes was about a few centimeters, and the size of the droplet was on the order of hundreds of micrometers.

In 2009, Ristenpart *et al.* discovered a phenomenon where in application of an electric field governs whether or not a changed droplet coalescences to the oppositely charged bulk water [32]. When the electric potential becomes higher than a threshold voltage, the droplet does not coalesce. This is not oscillation between the electrodes, but a closely related phenomenon. Having an understanding of the behavior of a charged droplet is useful for fields such as inkjet printing, mass spectroscopy, and cloud physics.

In 2010, Takinoue *et al.* reported the rotation of droplet rotating between diagonally arranged electrodes [33]. On the microscale, if we fabricate a machine according to conventional engineering approaches, it would be difficult to reproduce the desired motion because of the dominance of viscosity and friction. The abovementioned droplet rotation is a novel mechanism for driving microsized objects in such a scenario. Since 2010, many groups have reported on phenomena related to the oscillation of a droplet between the electrodes, as presented in Table 2.1.

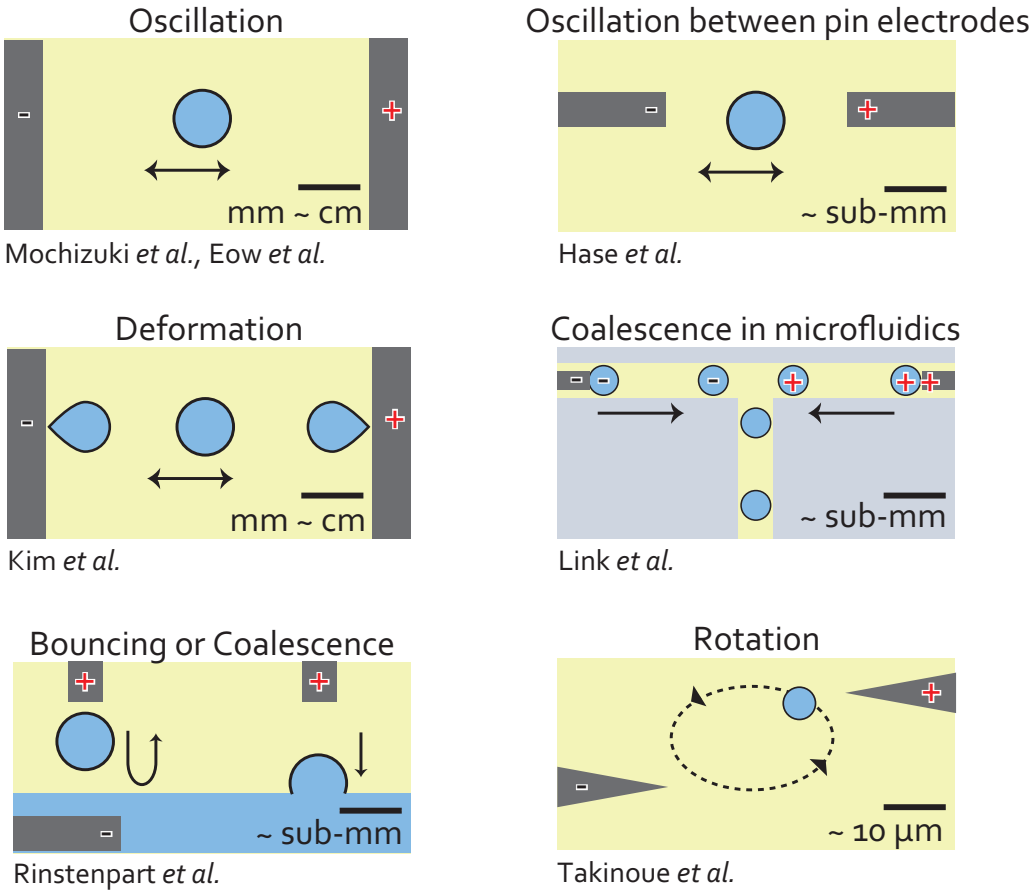

FIGURE 2.14: Schematic illustration of previous studies on oscillation of a droplet. Several study topics related to the oscillation of a conductive droplet in a dielectric liquid under an electric field.

TABLE 2.1: Recent studies (since 2010) on oscillation of a conductive droplet in dielectric liquid under electric field.

Group (year)	Purpose	Liquid of oil phase	Distance between the electrodes	Diameter and detergent of droplet
Im *et al.* (2011)[34]	Charging difference of liquids	KF-96(Silicon oil)	7.9 mm	250∼600 μm, water, milk and vinegar
Hamlin, Ristenpart (2012)[35]	Motion difference of surfactants	PDMS	6.5 mm	0.9 mm, water
Lee *et al.* (2012)[36]	Motion difference of the electrode position (near the oil-air surface)	KF-54/96	10 mm	1∼2 mm, water
Ahn *et al.* (2013)[37]	Motion difference of the electrode shape	KF-96	8 mm	250∼600 μm, water
Im *et al.* (2013)[38]	Application as digital microfluidics	PDMS	2.54 mm	$\sim$ 0.4 mm, water, $CaCl_2$+Alginate, $Na_2CO_3 + CaCl_2$
Kurimura *et al.* (2013)[1]	Motion difference of the distance between electrodes	Mineral oil	80∼150 μm	20∼50 μm, water
Mhatre *et al.* (2013)[39]	Using pin and plate electrodes	Castor oil, silicon oil	2.6 mm	400∼850 μm, water
Beranek *et al.* (2014)[40]	Application for microfluidics	Kerosene	500 μm	450 μm, water
Schoeler *et al.* (2014)[41]	Motion of O/W/O droplet	silicon oil	14 mm	800 μm, water/oil(O/W/O droplet)
Phan *et al.* (2014)[42]	Using two liquids have different pH instead of electrodes	Paraffin oil	1 mm	$\leq$ 1.2 mm, $FeCl_3$, NaOH, HCl, and NaCl
Drews *et al.* (2015)[43]	Using metal coated beads instead of droplet	Mineral oil	150 μm	14 μm, water

2.3.3 Droplet Charging

Most research groups have explained droplet motion in a manner similar to that described below and depicted in Fig. 2.15. First, the droplet attaches to the electrode, and it acquires some charges that are of the same sign as the electrode. The charged droplet is driven by the electric field. When the droplet reaches the other electrode, it acquires the charges that are of the same sign as the other electrode. The droplet then moves back toward the direction from where it came.

Some researchers have adopted charging models. For example, Mochizuki and Eow used the model of Felici and Cho [44]. Consder a charge denoted by Q; according to this model, it is expressed as

$$Q = \frac{1}{6}\pi r^3 \epsilon_1 \epsilon_2 E. \tag{2.34}$$

Here, r is the radius of the droplet; ϵ_1 and ϵ_2 are the dielectric constant of the particle/droplet and the medium, respectively; and E is the electric field. This model was also used by Khayari and Perez [25]. It assumes the droplet as the perfect conductor. Hase *et al.* also used this model; however, they considered the discharging of the droplet. Further, Takinoue *et al.* did not account for the explicitness of the model, they instead speculated that at the electrode, the droplet acquires some charges of the same sign as the electrode and that it loses charges in other areas. Jung *et al.* reported a difference between the model of Felici and Cho [44] and the charge estimated by them from their experimentally mesured droplet velocity.

We need to consider the governing equation for the charging of a dielectric liquid under an electric field.

2.3.4 Dielectrophoresis

In this section, we introduce the process of dielectrophoresis. Knowledge of this process is crucial to understanding the motion of a water droplet in oil under an electric field.

When a dielectric particle is placed in an electric field, dielectric polarization occurs on the particle, which causes the particle to act as the electric dipole. If the electric field is uniform, this dipole aligns to the direction of the field. However, when the droplet is placed in a nonuniform electric field, it drives the droplet. The force that drives the particle is called dielectric force [45], and it is described as

$$\boldsymbol{F}_{DEP} = 2\pi\epsilon_1 R^3 K \nabla \boldsymbol{E}^2. \tag{2.35}$$

Here, ϵ_1 and ϵ_2 is the dielectric constant of the medium and the particle, respectively; R is the radius of the particle; $\boldsymbol{E}$ is the electric field. K denotes the Clausius-Mossoti function, which is written as

$$K = \frac{\epsilon_2 - \epsilon_1}{\epsilon_2 + 2\epsilon_1}. \tag{2.36}$$

When the particle is the water droplet, $\epsilon_2 \sim 80$. The dielectric constant of oil is $\epsilon_1 \sim 2$. In this situation, $K > 0$. The direction of the dielectric force is as Fig. 2.16. Now, we consider the dielectric particle to be placed in uniform electric field $\boldsymbol{E}$. When the dipole

formed on the particle is denoted as $\boldsymbol{P}$, the relation between $\boldsymbol{E}$ and $\boldsymbol{P}$ is expressed as

$$\boldsymbol{P} = \alpha \boldsymbol{E}. \tag{2.37}$$

Here α is the macropolarizability. The force $\boldsymbol{F}$ that is applied to the particle under the electric field $\boldsymbol{E}$ is

$$\boldsymbol{F} = (\boldsymbol{P} \cdot \nabla)\boldsymbol{E}. \tag{2.38}$$

Then, upon substituting $\boldsymbol{P}$ in Eq. 2.37, we get

$$\boldsymbol{F} = (\alpha \boldsymbol{E} \cdot \nabla)\boldsymbol{E} \tag{2.39}$$

$$= (1/2)\alpha \nabla \boldsymbol{E}^2. \tag{2.40}$$

Here,

$$\nabla \boldsymbol{E}^2 = 2(\boldsymbol{E} \cdot \nabla)\boldsymbol{E} + 2\boldsymbol{E} \times (\nabla \times \boldsymbol{E}) \tag{2.41}$$

When there is no magnetic field, we can use $\nabla \times \boldsymbol{E} = 0$. Comparison of Eq. 2.35 and Eq. 2.40 gives

$$\alpha = 4\pi\epsilon_1 R^3 K. \tag{2.42}$$

When we consider a water droplet in an oil phase, we assume that the droplet has no charge. However, when there is a gradient of the electric field, the droplet can move because of dielectric force. The electric field does not have a gradient when parallel-plate electrodes are used.

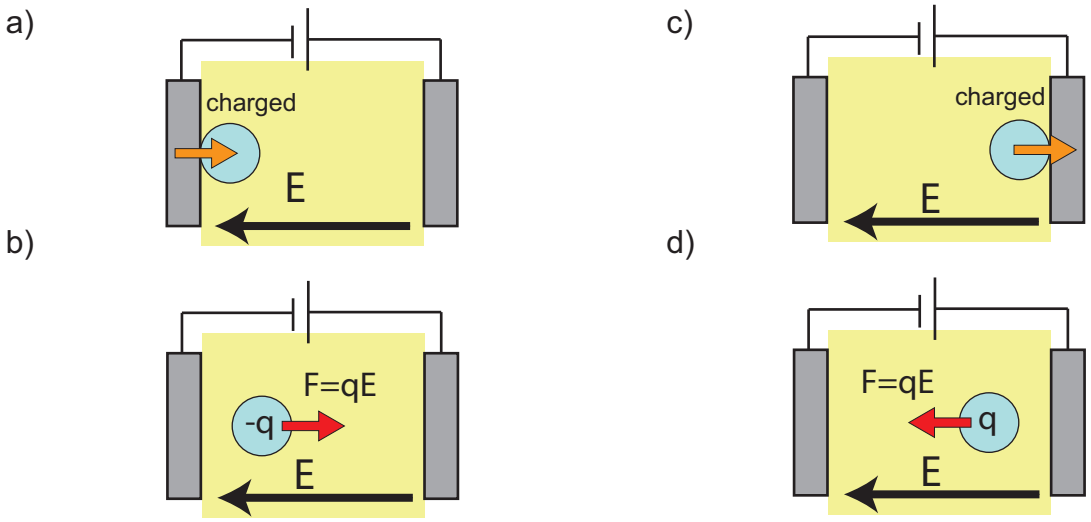

FIGURE 2.15: Schematic illustration of droplet oscillation. a) When the droplet attaches to the electrode, it acquires some charges. b) The charged droplet is driven by the electric field. c), d) The same phenomena as those seen in a), b) occur. The droplet exhibits the behaviors in a)-d) repeatedly.

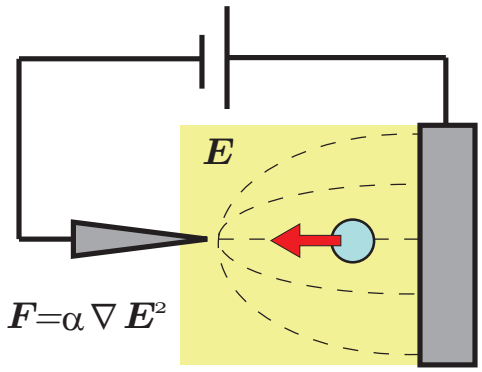

FIGURE 2.16: Schematic illustration of dielectrophoresis. The direction of the particle motion is determined by the ratio of the dielectric constant of the medium to that of the particle. When the particle is a water droplet and the medium is oil, the dielectric constant of the particle is larger than that of the medium. In this case, the droplet moves toward the direction in which $\boldsymbol{E}^2$ becomes larger.

2.3.5 Electrohydrodynamics

When a high voltage is applied to a dielectric liquid, it starts to flow. This phenomenon is termed EHD flow (Fig. 2.17(a)). When one electrode is inserted in a dielectric liquid and another is placed over the liquid, the liquid is observed to rise to the electrode as shown in Fig.2.17(b). This flow has potential applicability to EHD pumps and actuators. However, the mechanism of EHD flow is poorly understood. Two review papers of the EHD have been published: one in 1993 and the other in 2012. The latter paper includes only the detailed modeling of EHD flow.

When we use a completely dielectric liquid, it has low electric conductivity and permittivity. EHD flow is extremely slow. Recently, Ryu *et al.* [46] found that polar additives introduced in dielectric liquids enhance the EHD flow: they added Span 85 to dodecan solution and generated the EHD flow by application of ac voltage. In the latest review in 2012, the importance of dissociation and association in EHD flow has been reported.

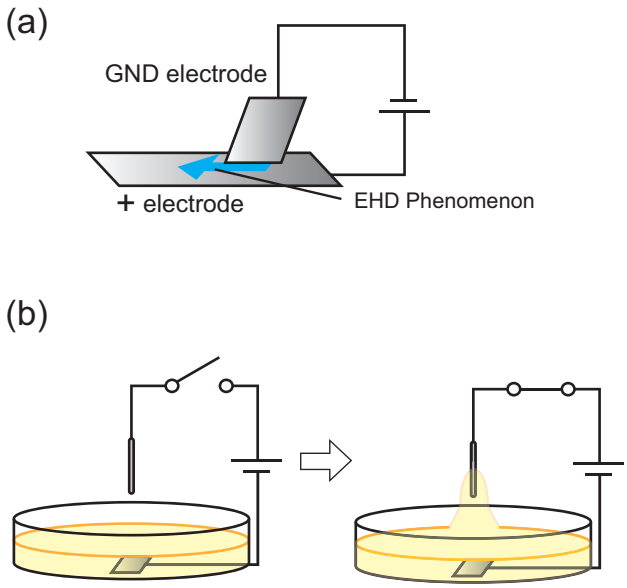

FIGURE 2.17: (a) Schematic illustration of EHD flow. When electric potential is applied to dielectric liquid, the liquid starts to flow. (b) Experiment on EHD. When a pair of electrodes is employed, the liquid is attracted to the electrode in air [47].

Chapter 3

Micro back-and-forth motion under DC electronic Field

3.1 Introduction

In Chapter 2, we introduced studies on a water droplet oscillating in an oil phase under a dc voltage. In the present work, we explore application of this droplet oscillator to nano- or micromachines. As mentioned in Chapter 1, the Reynolds number in a small-scale system is rather small, because of which it becomes necessary to establish a new methodology for fabricating nano- or micomachines. In the previous studies introduced in Chapter 1, application of an electrical potential on the order of 100 V was necessary to induce rhythmic or oscillatory motion where the distance between the electrodes was on the sub-millimeter scale. In the present chapter, we examine the effects of downsizing the experimental system and demonstrate that the critical voltage to induce oscillation of the droplet then decreases down to the level of 10 V. Interestingly, this decrease is not linear; rather, it exhibits dependence given by $\sim$1.5 power. This suggests that not only the electric field (V/L) but also the dielectric effects, i.e., ∇(V/L)2, have a decisive effect on the threshold voltage for inducing droplet oscillation. In addition, external noise enhances the oscillatory behavior as a kind of coherent resonance.

3.2 Experimental Setup

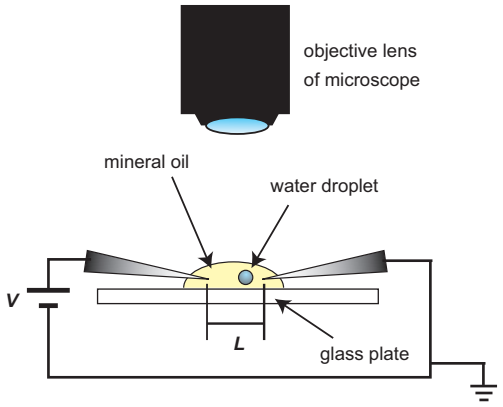

FIGURE 3.1: Schematic representation of the experimental setup. Stationary DC voltage was applied to the oil phase containing micro water droplets. V: Applied DC voltage. L: distance between the electrodes.

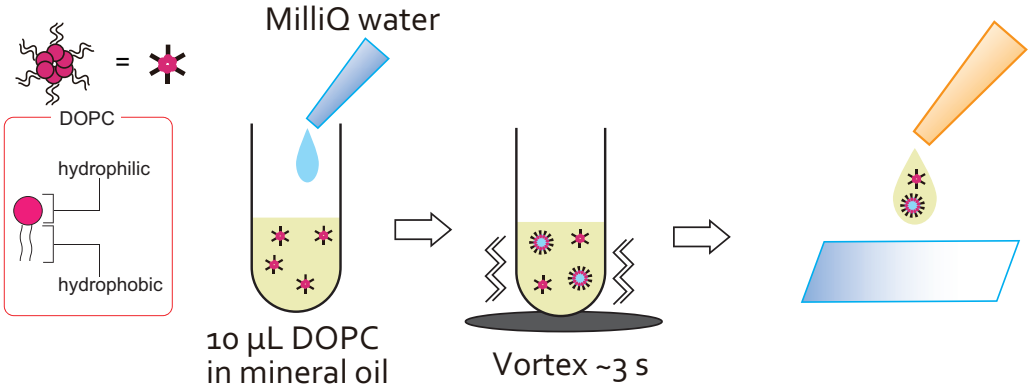

FIGURE 3.2: Schematic illustration of preparation of water droplet in oil phase. First, 10 μM DOPC was dissolved in mineral oil as a surfactant and sonicated properly. Next, 2 μL of MilliQ water was added to 10 μL of 10 μM DOPC in mineral oil. To generate a microsized droplet, a vortex mixer was run for around 3 s. Subsequently, the oil containing the water droplets was taken on a glass slide.

A schematic illustration of the experimental setup is shown in Fig. 3.1. A water droplet was suspended in mineral oil on a glass slide and direct current (DC) voltage was applied to the droplet using tapered tungsten electrodes. The motion of the droplet was observed using an optical microscope (KEYENCE VW-9000, Japan). To stabilize the micro-droplet, phospholipid molecules 10 μM dioleylphosphatidylcholine (DOPC) (WAKO, Japan) had been dissolved in mineral oil (Nacalai Tesque, Japan) by sonication for 90 min at 50 °C. 2 μl of pure water (Millipore, Japan) was added to 100 μl of the prepared mineral oil, and then the mixture was shaken by a vortex mixer for approximately 3 s to obtain w/o droplets (Fig. 3.2). In the present study, we have added phospholipid to stabilize the micro-sized water droplet [48], by considering the electro-chemical property that DOPC is zwitterion, *i.e.*, low electronic bias.

3.3 Results

Figure 3.3 shows typical examples of the oscillatory motion of a water droplet in a DC electric field between the tapered electrodes, with an increase in the applied voltage. The experiments show that the system exhibits a certain critical voltage for droplet oscillation, which is dependent on the distance between the electrodes. As shown in Fig. 3.3(a), at an inter-electrode distance of L = 210 μm, the droplet exhibited no apparent motion below a threshold voltage of 16.3 V where the voltage was gradually increased from 0 V to 16.3 V. When the applied voltage reached the threshold, the droplet started to oscillate between the edges of the electrodes. During this oscillatory motion as in Fig. 3.3, the voltage was fixed at the threshold value. The decrease in the distance between the electrodes to 140 μm resulted in a decrease in the threshold potential, as shown in Fig. 3.3(b).

A phase diagram of the droplet motion is denoted in Fig. 3.4 with threshold voltage values function of the distance between the electrodes. The results suggest that the threshold potential was almost independent of the size of the droplet. When the distance between the electrodes was below 70 μm, the droplets adhered to an electrode before or during voltage rising. The diagram indicates that the threshold voltage to

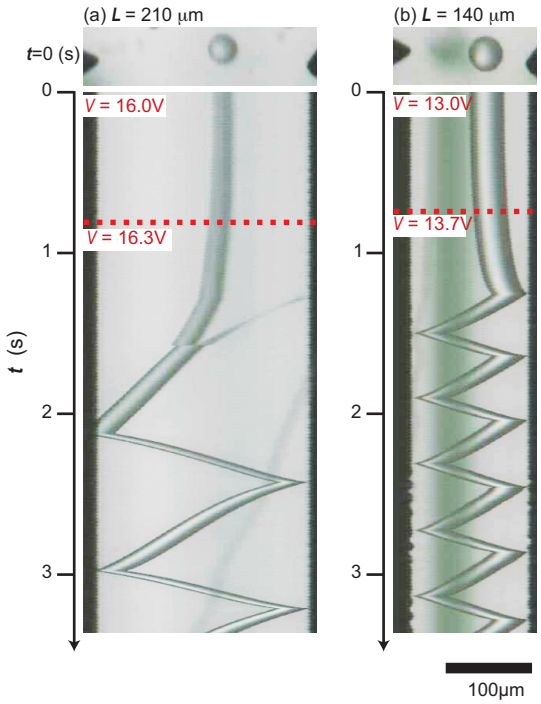

FIGURE 3.3: Spatio-temporal diagram of the motion of a droplet with a diameter of 34 μm at (a) L = 210 μm and (b) L = 140 μm. An increase in the applied DC voltage results in bifurcation from the static stationary to an oscillatory state.

cause the oscillation tends to diminish with the decrease of the counter-electrode distance, L. Notably, the threshold line exhibits nonlinear dependence, that is $V_c \sim L^{\gamma}$ where γ is 1.3 ± 0.2.

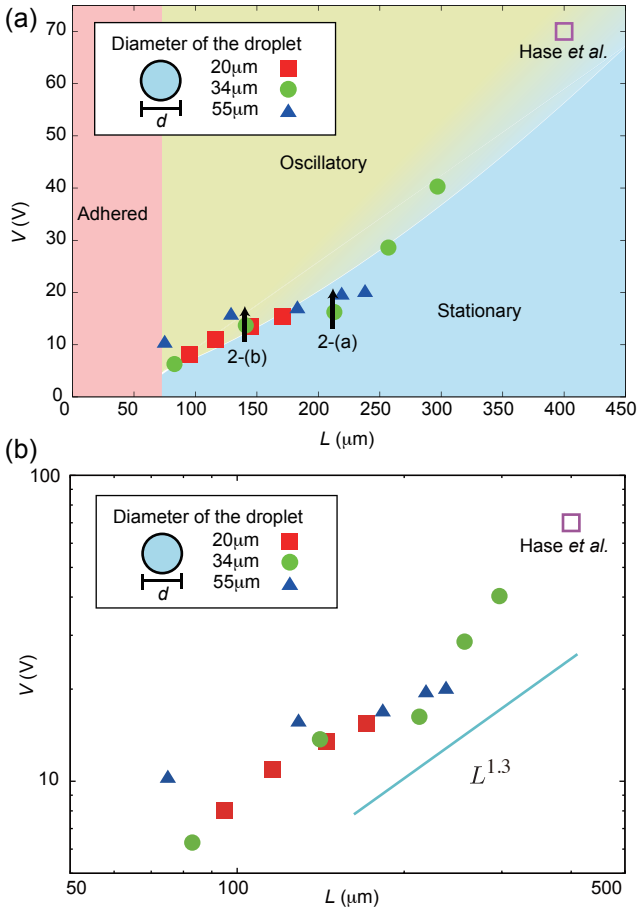

FIGURE 3.4: (a) Phase diagram for mode bifurcation between rhythmic motion and a stationary state as observed for droplets with different diameters, where each point represents the threshold value for bifurcation. The right top point is adapted from the last paper of our group [27]. The arrows correspond to the spatio-temporal behavior given in Fig. 3.3. (b) Plot of Log L vs Log V for the experimental data given in (a). The blue solid line is $L^{1.3}$, which is a best fit line to the experimental data.

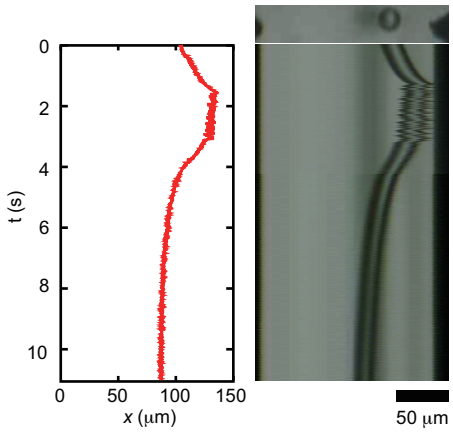

FIGURE 3.5: Spatio-temporal diagram (right) of the motion of a droplet together with the time trace of its center of mass (left) under the DC potential of 6 V. The droplet firstly moved toward the right electrode, then returned back, and finally stay still at the position near the middle of the couple of electrodes.

3.4 Numerical Simulation

Next, we discuss the underlying mechanism of the oscillatory motion with special emphasis on the effect of the distance between the electrodes, by adopting the simple phenomenological equation of motion:

$$k\dot{\boldsymbol{x}} = q\boldsymbol{E} + \alpha\nabla\boldsymbol{E}^2/2 \tag{3.1}$$

where k ($= 3\pi\eta d \sim 10^{-7}$ kg/s) is a coefficient of viscosity resistance, and $k\dot{\boldsymbol{x}}$ represents the viscosity resistance for a moving droplet with diameter d and velocity $\dot{\boldsymbol{x}}$. $q\boldsymbol{E}$ and $\alpha\nabla\boldsymbol{E}^2/2$ indicate the electric force and dielectric force, respectively acting on a droplet with charge q and polarizability α ($\cong 2\times10^{-11}$ $\mathrm{Nm^3/V^2}$) [45]. Under our experimental conditions, the Reynolds number is rather small; $Re = \rho u d/\eta \sim 10^{-3} \ll 1$, where ρ ($\sim 10^3$ $\mathrm{kg/m^3}$) and η ($\sim 10^{-3}$ $\mathrm{Pa\cdot s}$) are the density and viscosity of the mineral oil, respectively, and u ($\sim 10^{-4}$ m/s) and d ($\sim 10^{-5}$ m) are the velocity and diameter of the water droplet. As in Fig. 3.3, contribution of the inertia force is much smaller than that of the viscosity. We thus adapt the overdamped Langevin equation to interpret the droplet motion, by neglecting the inertial term in Eq. 3.1 for simplification. Now, we assume that the time-dependent change in the effective droplet charge, q. We put β is a coefficient that is associated with the electrostatic property and time scale. Then q is described as,

$$\dot{q} = \beta\frac{v}{l}\sinh(x) - \frac{q}{t_0} \tag{3.2}$$

Here, we put v as the voltage and l as the distance between the electrodes. The first term on the right hand in Eq. 3.2 (the hyperbolic sine term) represents the rapid charging effect for the droplet touching onto the electrode as a differentiable function by considering the symmetry of the experimental system. Through such kind of continuous function, we also incorporate the charging process for the droplet located near the electrode surface [27]. The second term in Eq. 3.2 indicates the gradual discharging effect during the translational motion of the droplet between the electrodes. In the past studies [27, 33], through the careful observation on gradual slowing down during the translational motion of the droplet, especially around the parameter region near the threshold between the oscillatory motion and the stationary states, it has been concluded that the slowing down is attributed to the discharging effect. In order to show the existence of the discharging effect, we exemplifies the observation on the slowing down as Figure 3.5, where the voltage between the electrodes was decreased to be 6 V before $t = 0$. This figure indicates the actual contribution of the discharging effect during the translational motion. The relaxation time is experimentally measured as 0.53 ± 0.18 s.

The electric field can be written as $\boldsymbol{E} = (E_x, E_y)$. From the geometrical characteristics in the experiment, we can regard that the electric field E_x along the direction between the tips of the electrode is almost constant, whereas the electric field E_y on the normal direction should be much large around the edges of the electrodes. To describe such spatial symmetry of E_y, we simply adapt the even power components, x^2 and x^4 are used as the lowest orders to interpret the observation as,

$$E_y^2 = (v/l)^2\left(-(x+1)^2(x-1)^2+1\right). \tag{3.3}$$

where the positions of the negative and positive electrodes correspond to $(x, y) =$

$(-1, 0)$ and $(x, y) = (1, 0)$, respectively. The general form of Eq. 3.3 is shown in Fig. 3.6. The detailed discussion about $E_y^2$is in Section 3.7.1. The effect of the distance between

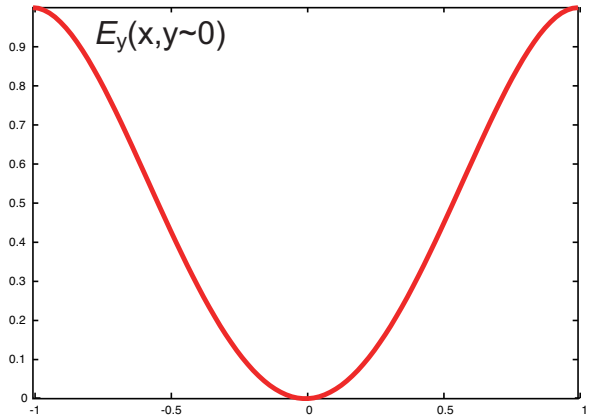

FIGURE 3.6: Schematic illustrations of the $E_y^2(x, y \sim 0)$.

the electrodes is taken in the coefficient. The x component in Eq. 3.1 can then be given as $k\dot{x} = qE_x + \alpha\partial_x E^2/2 \cong qE_x + \alpha\partial_x E_y^2/2 = qE_x - (2\alpha v^2/l^3)x(x+1)(x-1)$,

$$\dot{x} = \quad E_x q/k - (2\alpha v^2/kl^3)x(x+1)(x-1). \tag{3.4}$$

For simplification, we set $E_x = -v/l$, since a droplet moves on the line between the electrodes during back-and-forth motion. Then Eq. 3.4 is given in a dimensionless form as,

$$\dot{x} = \quad -qv/kl - (2\alpha v^2/kl^3)x(x+1)(x-1). \tag{3.5}$$

The qualitative behavior of $\dot{x}$ is dominated by the balance between the dielectric and electrostatic terms.

Figure 3.7 shows typical results of the numeric calculation with the coupled differential Eqs. 3.2 and 3.5, by mimicking the experimental condition in which the voltage is gradually increased. In this regime, an increase in the voltage forces the droplet away from $x = 0$ to exhibit oscillatory motion. The electrical field, v/l, in Fig. 3.7(a) is greater than that in Fig. 3.7(b). The frequency of the back-and-forth motion of the droplet increases in proportion to an increase in the electric field between the electrodes.

Figure 3.8 shows a phase diagram of the numerical simulation. The schematic illustration of the phase field of each region I, II, and III is illustrated as Fig. 3.9. Regions I and II exhibit a stable fixed point at $x = 0$ and the limit cycle, respectively. The stationary region I and the oscillatory region II exhibit a boundary line with $v_c = \sqrt{kl^3/t_0\alpha}$, which roughly corresponds the boundary curve in the experiment. As shown in both experiment and numerical simulation, the transition from stationary to oscillatory phase is not proportional to L, but to $3/2$ on the power of L as calculated in linear stability analysis around stable fixed point [14]. The least square fitting on the present experimental results as given by $L^{3/2}$ relationship is extrapolated well to the data point reported by Hase *et al.* [27], as is revealed in Fig. 3.3. Competition between the dielectric force and the static electric forces causes the limit cycle in terms of the nonlinear dynamics and this bifurcation. It should be noted that such kind of bifurcation is generated only for smaller length scale. In larger system, the relative importance of the

effects change significantly accompanied by the decrease on the dielectric contribution and increase on the inertia.

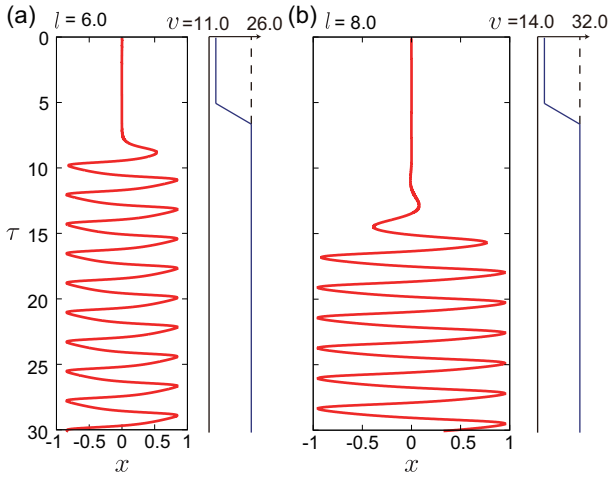

FIGURE 3.7: Spatio-temporal diagram deduced from the numerical calculations based on Eqs. 3.2 and 3.5, where $t_0 = 0.6, \alpha = 0.075, \beta = 0.025, k = 0.4$. The corresponding value of voltage, v, changes linearly as in the graph beside the $x - \tau$ diagram. The distance between the electrodes is $l = 6.0$ in (a), $l = 8.0$ in (b). The applied voltage is changed from $v = 11.0$ to $v = 26.0$, whereas in(b), the voltage is from $v = 14.0$ to $v = 32.0$, as shown in the time-traces shown on the right. The time (τ) and space (x) scales are arbitrary.

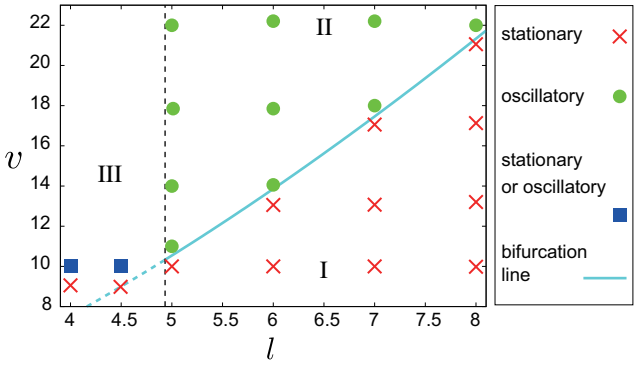

FIGURE 3.8: Phase diagram showing the numerical results with changes in l and v. The parameters are $t_0 = 0.6$, $\alpha = 0.075$, $\beta = 0.025$, $k = 0.4$. v and l are dimensionless variables. At the open circles, the droplet exhibits oscillatory motion. At the filled circles, oscillatory and stationary states coexist. At the cross marks, the droplet falls to the fixed point $x = 0$. At the square, the droplet is trapped at fixed points near the electrodes or it oscillates. It depends on the initial condition.

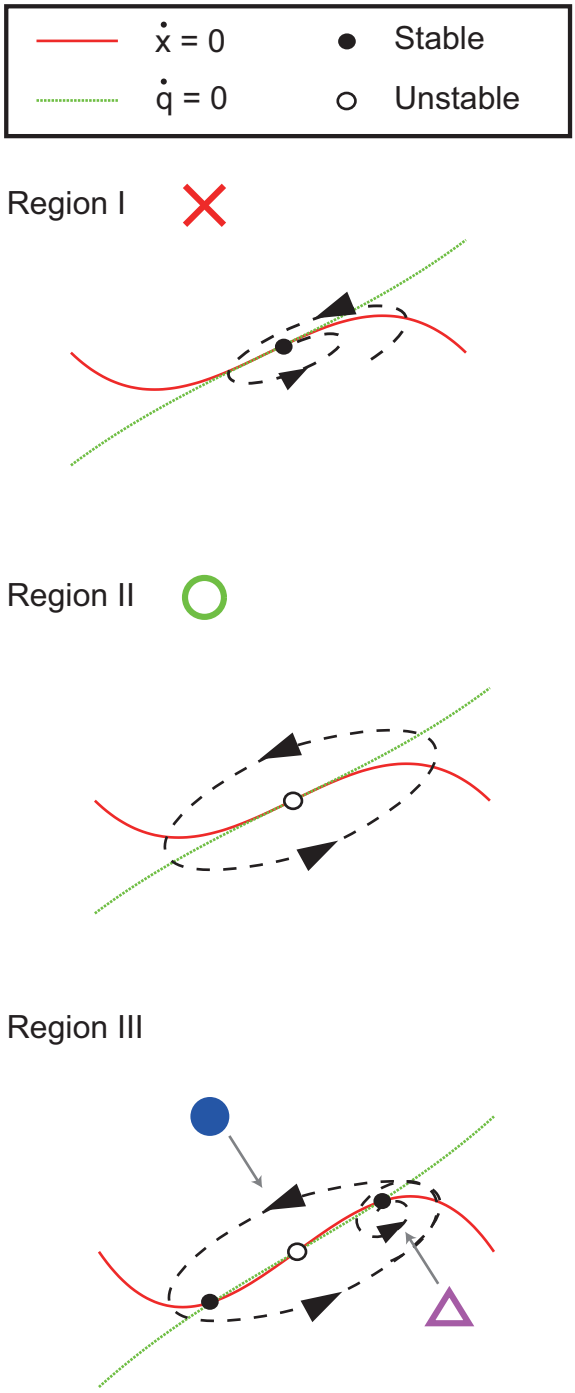

FIGURE 3.9: Schematic illustrations of the phase field of each region corresponds to Fig. 3.8.

3.5 Discussion

The results of the numerical simulations thus has reproduced the essential aspects of the experimental observations, including the scaling law on the bifurcation. Here, we should mention that there exists some degree of discrepancy on the simulation from the actual droplet motion near the electrodes. Such discrepancy is attributable to the simple assumption in our numerical model, where the potential is represented only with x^2 and x^4 terms, in order to grasp the essence of the oscillatory phenomena. It is highly expected that the behavior of the droplet near the electrode would be more precisely described by adapting the physico-chemical properties as reported for a metal sphere [25] and also for a liquid sphere [34].

Region III exhibits a pair of attractive fixed points near the electrodes, however, it is difficult to identify the fixed points in region III due to the adhesive behavior of the droplet on the electrode under lower voltage in the experiment. Although we have discussed the behavior around the boundary between regions I and II, the position of droplet is not strongly confined because the trapping potential is broad around the fixed point in the stationary region I. This fact is also observed in the experiments, where the observed positions of the trapped droplet are dispersed. Therefore, the addition of pulses or noise with a certain strength can create large motion even in the stationary region I. In addition, we can also apply pulses or noise to induce effective oscillations in the stationary region III. This feature corresponds to a coherent resonance with a bistable velocity field with excitability, where the inherent bistability comes from dielectric trapping near the electrodes.

To examine the above mentioned effect of noise, we performed the experiment with external noise. Although noise can be present in force, charge, voltage, and so on, in this experiment we could control the noise in voltage. Therefore Gaussian white noise of 500 kHz bandwidth was applied on the electric potential. With a reduction in the DC electric potential, the frequency of oscillation became intermittent. In the typical demonstration shown in Fig. 3.11, the droplet stopped near the electrode under 5 V (showed as Fig. 3.10). When the Gaussian noise was added to the DC potential, where the offset was 5 V and peak-to-peak was 1 V, the droplet started to oscillate again. This behavior is similar to the numerical calculation with noise although the dielectric trapping or adhesion on the electrodes must be larger than that in the numerical equation. In other words, the experiment clearly exhibits a characteristic of coherent resonance [16] in an excitable system. It is, therefore, expected that the parameter area of the oscillation is expanded under noisy environment.

Finally, we would briefly mention the effect of surfactants. Since we adapt relatively small droplets, the effect of the morphological deformation was negligible small under our experimental conditions. However, detergents such as Triton X-100 and Span 85 caused obvious deformation of the droplet under DC voltage: It may be an interesting extension to examine the effect of deformation coupled with the oscillatory motion.

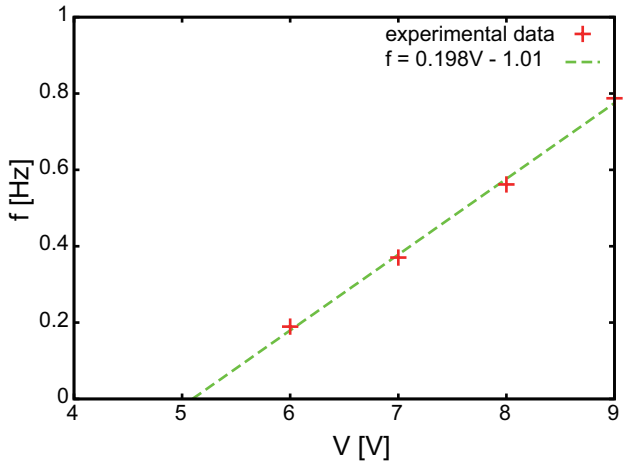

FIGURE 3.10: Relation between the voltage and the frequency of the droplet oscillation. The points are the experimental results and the broken line is the linear fitting.

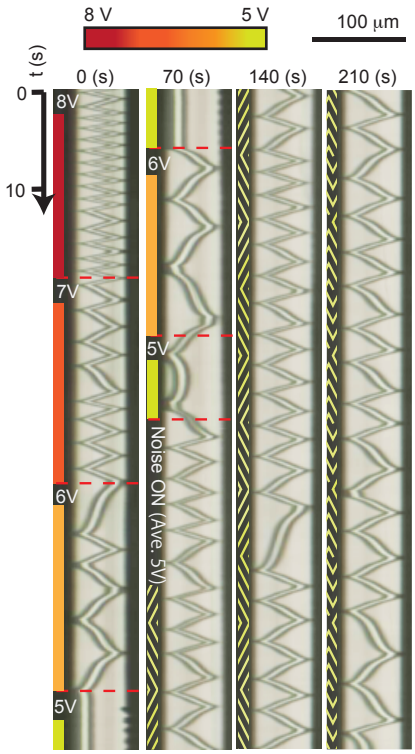

FIGURE 3.11: Spatio-temporal diagram of the motion of a droplet with a diameter of 24 μm at L=56 μm. For the period from t = 0 to t = 100 s, the stationary DC voltage is decreased in a stepwise manner as shown in the figure. From t = 100 s, we started adding the noise to DC 5 V.

3.6 Conclusion

In conclusion, we have demonstrated that sustained rhythmic motion between a pair of electrodes is generated under DC voltage on the order of several volts through downsizing to the order of 10 μm. We propose a phenomenological model equation and reproduce the essential behavior of the droplet motion. Significant effect of noise against the stationary region is observed both in the experiments and the simulation, where the noise promotes the occurrence of rhythmic motion of the droplet.

3.7 Supplemental Discussion

3.7.1 Functional form of E_y

In this time, we used the estimated functional form as E_y. We can not derive the analytically E_y. To examine the shape of E_y, we calculate it numerically.

The schematic representation of Eq. 3.3 is shown as Fig. 3.12. The value of E_y near

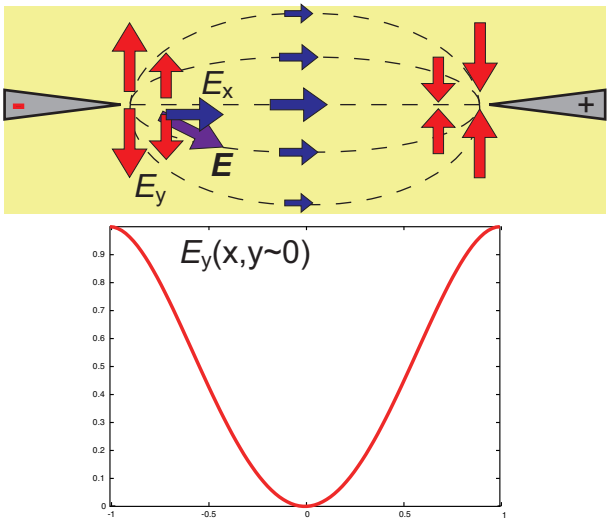

FIGURE 3.12: Schematic illustration of the electrical field in out experiment.

the electrodes is higher than the other region.

Next, we did the numerical calculation with using the finite element method software COMSOL Multiphysics. The result is shown in Fig. 3.13. The triangles in the right and left side represent the electrodes. The potential of right triangle is 1 and that of the left is 0. The red vector represents the electrical field. The rainbow lines are the equipotential lines. The tendency of the magnitude and direction of red vectors is the same the arrows in Fig. 3.12.

From the numerical calculation, we thought $E_y(x, y \sim 0)$ can resemble as

$$\left(-((x/L)+1)^2((x/L)-1)^2+1\right). \tag{3.6}$$

Eq. 3.3 is the non-dimensional form of Eq. 3.6.

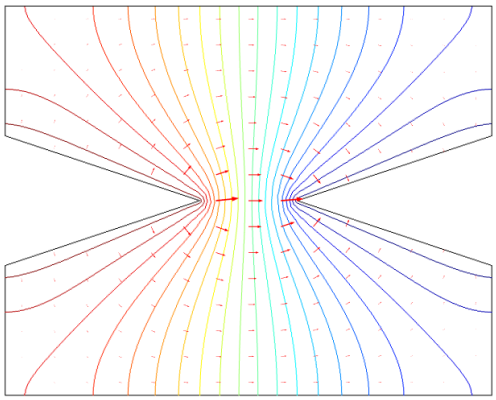

FIGURE 3.13: Result of numerical calculation of the electric field by the software(COMSOL Multiphysics). The red vector represents the electrical field. The rainbow lines are the equipotential lines.

3.7.2 Details of model

In this section, we discuss the numerical model more precisely.

At first, we have a equation of motion 3.1 as

$$k\dot{\boldsymbol{x}} = q\boldsymbol{E} + \alpha\nabla\boldsymbol{E}^2/2. \tag{3.7}$$

Here, k is the viscosity coefficient, $\boldsymbol{x} = (x, y)$ is the displacement of the droplet, $\boldsymbol{E} = (E_x, E_y)$ is the electric field, q is the charge of the droplet. In this time, we only think about the x-displacement of the droplet.

We at first think the positions of the tips of electrodes are $(x, y) = (l/2, 0)$ for the plus electrode and $(x, y) = (-l/2, 0)$. Then distance between the electrodes is l. For the static electric force, we think the droplet is as a point $q\boldsymbol{E} \sim qE_x$. We consider $E_x = -v/l$. The term of dielectric force, the 2nd term in the right hand of Eq. 3.1, is derived from the gradient of E_y. This is because we consider that E_x does not change along x. We can not determine E_y under the geometry of the experiment analytically, then we use

$$E_y^2 = (v/l)^2\left(-(\frac{x}{l/2}+1)^2(\frac{x}{l/2}-1)^2+1\right). \tag{3.8}$$

We substitute Eq. 3.8 to Eq. 3.1, Equation 3.1 comes out

$$\begin{aligned} k\dot{x} &= qE_x + \alpha\partial_x E^2/2 && (3.9)\\ &\cong qE_x + \alpha\partial_x E_y^2/2 && (3.10)\\ &= -qv/l - 2\alpha\frac{v^2}{l^3}\times\frac{x}{l/2}(\frac{x}{l/2}+1)(\frac{x}{l/2}-1). && (3.11)\end{aligned}$$

Here, we set $x' = x/(l/2)$, then

$$k(l/2)\dot{x'} = -qv/l - 4\alpha\frac{v^2}{l^3}\times x'(x'+1)(x'-1). \tag{3.12}$$

Finally we get the equation of motion as

$$k\dot{x'} = -2qv/l^2 - 8\alpha\frac{v^2}{l^4}\times x'(x'+1)(x'-1). \tag{3.13}$$

We also modify the equation of charge as

$$\dot{q} = \beta\frac{v}{l}\sinh(x/(l/2)) - \frac{q}{t_0}. \tag{3.14}$$

$t = 0$ is the relaxation time of discharging. We as well set $x' = x/(l/2)$, then

$$\dot{q} = \beta\frac{v}{l}\sinh(x') - \frac{q}{t_0}. \tag{3.15}$$

Therefore, the equations the droplet follows are

$$\begin{aligned} k\dot{x'} &= -2qv/l^2 - 8\alpha\frac{v^2}{l^4}\times x'(x'+1)(x'-1), && (3.16)\\ \dot{q} &= \beta\frac{v}{l}\sinh(x') - \frac{q}{t_0}. && (3.17)\end{aligned}$$

Number of the fixed points

Firstly, we derive number of the cross points of $f(x)$ and $g(x)$.

For Eqs. 3.13 and 3.15, we put $\dot{x'} = 0, \dot{q} = 0$, then we get,

$$0 = -2qv/l^2 - 8\alpha\frac{v^2}{l^4} \times x'(x'+1)(x'-1) \quad \Leftrightarrow q = 4\alpha\frac{v}{l^2}x'(x'+1)(x'-1), \tag{3.18}$$

$$0 = \beta\frac{v}{l}\sinh(x') - \frac{q}{t_0} \quad \Leftrightarrow q = \beta t_0\frac{x}{l}\sinh(x'). \tag{3.19}$$

We define as

$$q = 4\alpha\frac{v}{l^2}x'(x'+1)(x'-1) \equiv f(x), \tag{3.20}$$

$$q = \beta t_0\frac{x}{l}\sinh(x') \equiv g(x). \tag{3.21}$$

The slopes of $f'(x=0)$ and $g'(x=0)$ define the number of the fixed points. $f'(x=0)$ and $g'(x=0)$ are

$$f'(x=0) = -4\alpha\frac{v}{l^2}, \tag{3.22}$$

$$g'(x=0) = -\beta t_0\frac{x}{l}sinh(x'). \tag{3.23}$$

When $f'(x=0) = g'(x=0)$,

$$l = 4\alpha/(t_0\beta) \equiv l_0. \tag{3.24}$$

If $l > l_0$, $f(x)$ and $g(x)$ has only one cross point. The cross point is $x = 0$. Otherwise, $f(x)$ and $g(x)$ have three cross point, $x = 0$ and $x = x_0, -x_0 (x_0 \neq 0)$.

These cross points of $f(x)$ and $g(x)$ are the cross points of $dx/dt = 0$ and $dq/dt = 0$. Therefore we can think the cross points as the fixed points.

Stability around the fixed point

Next, we check the stability of the fixed point. Here we take the fixed point $(x, y) = (x_0, q_0)$ and think the small displacement $\delta x, \delta q \gg 1$. The equations of $\delta x, \delta q$ can be linearized, then we get $f(x), g(x)$ as

$$\frac{d}{dt}\begin{pmatrix}\delta x\\ \delta q\end{pmatrix} = \begin{pmatrix}-4\alpha v^2(3x_0^2-1)/kl^3 & -v/kl\\ -(\beta v/l)\cosh(x_0) & -1/t_0\end{pmatrix}\begin{pmatrix}\delta x\\ \delta q\end{pmatrix} \tag{3.25}$$

We represent the matrix on the right hand as $\boldsymbol{A}$. We also decide

$$\boldsymbol{A} = \begin{pmatrix}a & b\\ c & d\end{pmatrix}$$

$$tr\boldsymbol{A} = a + d, det\boldsymbol{A} = ad - bc.$$

The time-development of δx is written as $e^{\lambda t}$, here

$$\lambda = \frac{tr\boldsymbol{A} \pm \sqrt{(tr\boldsymbol{A})^2 - 4det\boldsymbol{A}}}{2}. \tag{3.26}$$

If δx oscillates,

$$(tr\boldsymbol{A})^2 - 4det\boldsymbol{A} < 0. \tag{3.27}$$

Assuming that δx oscillates, the condition that the fixed point is stable is $tr\boldsymbol{A} < 0$. Otherwise δx is amplified.

Now, we think the fixed point as $x_0 = 0$. The bifurcation point is considered as

$$tr\boldsymbol{A} = \frac{8\alpha v_c^2}{kl^4} - \frac{1}{t_0} = 0 \tag{3.28}$$

The voltage v_c means the threshold voltage and represent as

$$v_c = \sqrt{\frac{kl^4}{8t_0\alpha}} \tag{3.29}$$

The condition of oscillation is Eq. 3.27. When $x_0 = 0$, Eq. 3.27 becomes

$$(tr\boldsymbol{A})^2 - 4det\boldsymbol{A} = \left(8\alpha\frac{v^2}{l^4} - \frac{1}{t_0}\right)^2 - 4\left(8\alpha\frac{v^2}{l^4t_0} - \frac{2v^2\beta}{l^3}\right). \tag{3.30}$$

The first term in the right hand is plus. If we show the second term is plus, $(tr\boldsymbol{A})^2 - 4det\boldsymbol{A}$ is plus.

$$4\left(8\alpha\frac{v^2}{l^4t_0} - \frac{2v^2\beta}{l^3}\right) < 0 \tag{3.31}$$

is one of the conditions. By simplifying this, we get $l > 8\beta t_0/\alpha$.

Scaling of model

Now, we think the scaling of the model equations Eqs. 3.13 and 3.15. We use the dimensionless constant L for length, T for time and Q for charge and V for voltage. The dimensionless variable is written with $'$. x' has already normalized.

$$k(1/T)\dot{x'} = -2(QV/L^2)q'v'/l'^2 - 8\alpha(V^2/L^4)\frac{v'^2}{l'^4} \times x'(x'+1)(x'-1), \tag{3.32}$$

$$\Leftrightarrow k(L^2/VQT)\dot{x'} = -2q'v'/l'^2 - 8\alpha(V/L^2)\frac{v'^2}{l'^4} \times x'(x'+1)(x'-1) \tag{3.33}$$

$$(Q/\dot{T})q' = \beta(V/L)\frac{v'}{l'}\sinh(x') - \frac{Qq'}{Tt'_0} \Leftrightarrow \dot{q'} = \beta(V/TQL)\frac{v'}{l'}\sinh(x') - \frac{q'}{t'_0}. \tag{3.34}$$

Here we decide $T = 1$ and

$$k' = k(L^2/VQ) \tag{3.35}$$

$$\alpha' = \alpha(V/L^2) \tag{3.36}$$

$$\beta' = \beta(V/QL), \tag{3.37}$$

Then equations 3.33 and 3.34 becomes

$$k'\dot{x'} = -2q'v'/l'^2 - 8\alpha'\frac{v'^2}{l'^4} \times x'(x'+1)(x'-1) \tag{3.38}$$

$$\dot{q'} = \beta'\frac{v'}{l'}\sinh(x') - \frac{q'}{t'_0}. \tag{3.39}$$

These are the same equations as 3.33 and 3.34.

k is the viscosity coefficient. We think it follows Stokes' law, then

$$k = -6\pi\eta r. \tag{3.40}$$

η is the viscosity of oil $\sim 10^{-3}$ (Pa $\cdot$ s). α is introduced as $\alpha = 4\pi\epsilon_1 r^3 K$. ϵ_1 is the dielectric constant of water ~ 80. $K = \epsilon_2 - \epsilon_1/\epsilon_2 + 2\epsilon_1$ and ϵ_2 is the dielectric constant of oil ~ 4. Here we decide $r \sim 10^{-5}$ then we get $k \sim 10^{-7}$ and $\alpha \sim 10^{-13}$. β is the parameter in our model and we cannot decide by using the real value.

Fitting of experimental data

We try to fit the experimental data (Fig. 3.4(b)). With using the fitting function of gnuplot, we first decided the power of the distance between the electrdes l. As we described in the main part, the dependence of L is 1.3. From this result, we think the first model we described in the main part is more suitable than modified one. In the modified model, we scale the E_y function (Eq. 3.3) with l. If the former model is correct, the function of E_y does not change when we change the distance between electrodes. This is reasonable when we consider the effect of the tapered electrode. When the distance between the electrodes becomes wider, the elecrical field near the electrode does not change dramatically. Then we use the first introduced model for fitting. When we fit the results by using the function $f(x) = a * L^{3/2} + b$, we get the coefficients as $a = 0.060 \pm 0.00069$ and $b = 3.0 \pm 1.8$.

Secondly, we are going to make Eq. 3.1 non-dimensional form,

$$\frac{kL}{QV}\dot{x} = -q\frac{v}{l} - \frac{\alpha V}{L^2}\frac{2v^2}{l^3}x(x+1)(x-1). \tag{3.41}$$

Here, we put $\alpha' = (\alpha V)/L^2$ and $k' = (kL)/(QV)$. When we decide $L = 25 \times 10^{-6}$, $V = 1.0$ and the parameters we use in the numerical simulation are $\alpha' = 0.025$ and $k' = 0.4$, α becomes 25×10^{-13}. This value of α corresponds to the value when the water droplet is about 30 μm. We can not decide k and Q independently. When the droplet is about 30 μm, k becomes 5.6×10^{-7}. Using this value of k, we get Q as 3.5×10^{-12}. Since the order of q, the charge in numerical calcuration, is about 0.01, the order of charge in the experiments becomes 10^{-14} C. The other group measured the charge of the droplet as 10^{-9} C. However, our scale of the experiment is smaller than theirs. Thus we can think this is reasonable.

When we calculate the coefficient of $L^{3/2}$ with using these constants, we get 0.02. The order of the coefficient agree with that we get from fitting.

There are two assumed reason for this difference. One is that the surfactant makes the drag coefficient k larger. When there are surfactants on the surface between a droplet and surrounded liquid, the effective drag coefficient is larger than Stokes' law [49]. The second reason is that the surfactant make the dielectric constant of oil higher. There are many micelles of surfactant in an oil phase. According to $\alpha = 4\pi\epsilon_1 r^3 K$ and

$K = (\epsilon_2 - \epsilon_1)/(\epsilon_2 + 2\epsilon_1)$, ϵ_1 is the dielectric constant of water and ϵ_2 is that of oil. When ϵ_2 becomes larger and close to ϵ_1, K becomes smaller. Then α also becomes smaller, the coefficient becomes smaller.

Chapter 4

Noise-supported actuator: Coherent resonance in the oscillations of a micrometer-sized object under a dc-voltage

4.1 Introduction

We succeeded the downsizing of the droplet oscillator in an oil phase under dc voltage in Chapter 3. We also indicate noise can broaden the region of oscillation. This means the droplet can oscillate under the threshold voltage by adding noise. This stability for a noisy environment is suitable for making the nano- or micro-sized machine. Because we can not neglect the effect of thermal fluctuation when the system size becomes nano to a few micron order.

In the present chapter, we confirm that for noise strength the noise-triggered motion shows resonance behavior as a consequence of coherent resonance of the limit-cycle oscillation. We believe this noise-supported actuation of the small object through this sustained and robust oscillation will be a key technology in constructing nano-actuators working under strong thermal fluctuations or mimicking biological molecular motors [10, 50].

4.2 Material and Methods

A schematic illustration of the experimental setup (Fig. 4.1) shows a size-selected water droplet suspended in mineral oil on a glass substrate. The direct current (dc) voltage with Gaussian white noise (500 kHz bandwidth) was applied to a pair of tapered tungsten electrodes immersed in the oil. To stabilize the micro-droplet, phospholipid molecules 100-μM dioleoylphosphatidylcholine (DOPC, Wako, Osaka, Japan) was dissolved in the mineral oil (Nacalai Tesque, Kyoto, Japan) through sonication for 90 min at 50 °C. DOPC works as a weak surfactant with zwitterions, i.e., neutral molecules with a low electronic bias. During droplet preparation, 2 μL of pure water (Millipore, Japan) was added to 100 μL of the mineral oil, and then the mixture was shaken by a vortex mixer for approximately 3 s to obtain water-in-oil emulsion droplets. The dc voltage with noise was generated by a function generator (WF 1974, NF Corp, Yokohama, Japan), then magnified by a voltage amplifier (POS 60-2.5, Matsusada, Shiga, Japan). A resistor of resistance (R=10 MΩ) was placed in series with the electrodes. The motion of the droplet was observed using an optical microscope (VW-9000, Keyence,

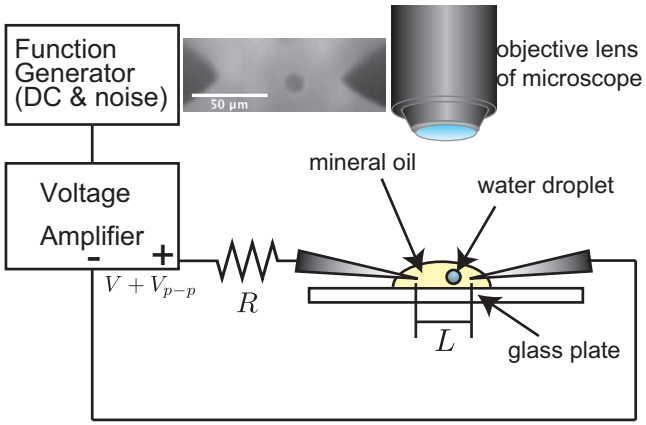

FIGURE 4.1: Schematic representation of the experimental setup. L is the distance between the electrodes. The function generator outputs a dc bias voltage and voltage noise; the combined signal is then magnified by the voltage amplifier.

Osaka, Japan), and then the acquired images were processed and analyzed through MATLAB software.

We first confirmed the threshold point without noise for the oscillations of a droplet between the electrodes. The threshold point depends on droplet size and electrode separation [1], but was almost constant for an individual droplet during the series of experiments. A typical result for threshold is shown in Fig. 4.2, where the droplet stops around 35.8 to 41.8 V as the voltage was decreased. Next, we added various noise signals to the applied voltage with the droplet stationary in a dc voltage of 35.8 V just below the threshold. In this instance, the largest amplitude of the noise was constrained to 41.8 V_{p-p} by the amplifier and the function generator. This V_{p-p} value of the noise corresponds to a peak-to-peak value of a Gaussian distribution, which determines the distribution of noise amplitudes. Note that the mean square value of the noise amplitude was much smaller. We maintained the value of the electric potential for a while and then decreased the noise amplitude for measurements.

4.3 Results

Figure 4.2 shows the initial stage of the time evolution of the droplet position. The centroid of the binarized image of the droplet was traced. With a noise amplitude of 41.8 V_{p-p}, the droplet stayed for long periods near the center between the electrodes. Nevertheless, the droplet oscillated strongly when the noise was decreased by 23.7 V_{p-p}. However, under the smaller amplitude of 5.8 V_{p-p}, the droplet exhibited small fluctuations near one of the electrodes (bottom panel of Fig. 4.2). In these experiments, oscillatory behaviors were frequently seen at moderate noise amplitudes.

4.4 Analysis

At first, we did the short-time Fourier transformation (SFFT) to capture the essentials observed with this phenomenon. The results of Short-time Fourier transformation was

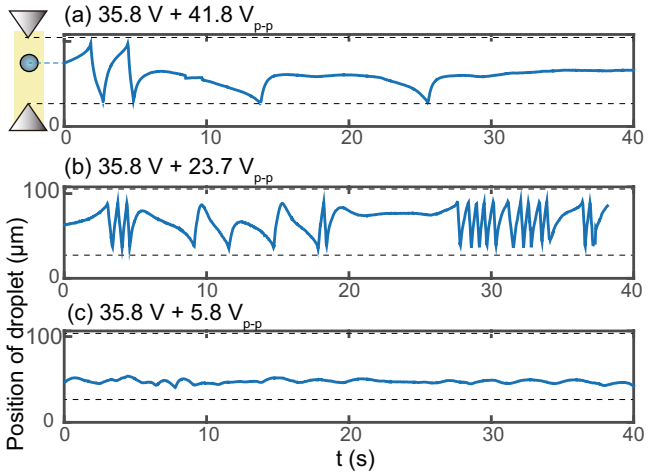

FIGURE 4.2: Time evolution of the droplet position. The voltage from the amplifier is (a) 35.8 V + 41.8 V_{p-p}, (b) 35.8 V + 23.7 V_{p-p}, (c) 35.8 V + 5.8 V_{p-p}. The position of the droplet was measured along the axis between the electrodes. The positions of the electrode tips, indicated by broken lines, are 104 and 24 μm.

not so clear that we decide to use continuous wavelet transformation (CWT). The detailed description is written in Appendix A.

Then, we applied CWT analysis to the time-series data.

To capture the essentials observed with this phenomenon, we applied continuous wavelet transformation (CWT) analysis to the time-series data.

$$C(a,b;f(t),\psi(t)) = \int_{-\infty}^{\infty} f(t)\frac{1}{\sqrt{a}}\psi^*(\frac{t-b}{a})dt, \tag{4.1}$$

which expresses the coefficient of the CWT where $f(t)$ denotes the signal, and a and b are constants. $\psi^*(t)$ is the complex conjugate of $\psi(t)$, which is the mother wavelet of Symlet. The constant a ranged from 1 to 128, whereas b was set as the number of data points. The sampling intervals of the data points are set at 1/30 s (droplet motion) and 0.02 s (noise). In calculating the CWT of a signal $f(t)$, one obtains a map of the coefficient $C(a,b;f(t),\psi(t))$ which can be displayed as a two-dimensional plot of a and b. To extract the relative intensity of the oscillatory motion from the map, we integrate the map along the time b and normalized (divided) by b. Finally, the time-averaged coefficient as a function of frequency or cycle was obtained.

Figure 4.4 shows the CWT spectra of the time series data for the voltage applied across the electrodes immersed in the oil solution without droplets. An oscilloscope was used in measuring this voltage. We confirmed the applied noise behaved as Gaussian white noise. From Fig. 4.4(a), each curve for the applied voltage exhibits a near-flat trend except near the end of the spectra for which the narrow peak at 4.9 Hz is an artifact of the analysis. White noise is thus being applied and contains almost all frequencies in the range of the present time scale of the droplet motion. Figure 4.4(b) also shows the voltage distribution of the noise determined as deviations from the dc bias value. Bin loses are due to mismatches between the oscilloscope and amplifier

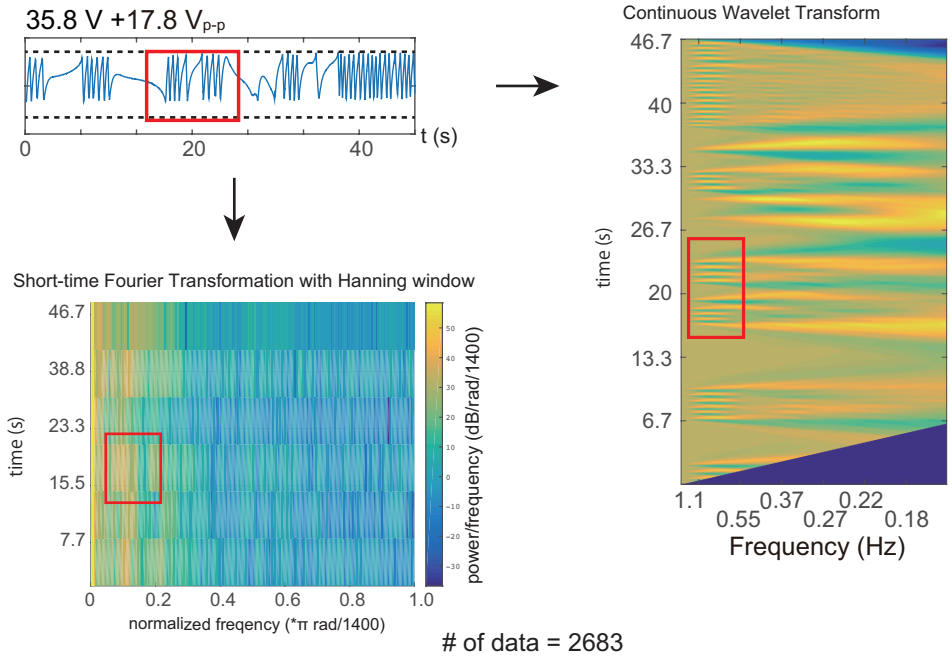

FIGURE 4.3: Comparing the CWT analysis with the Shot-time Fourier transformation (SFFT). The result of CWT indicates the characteristic oscillation better than SFFT.

resolutions, where the sampling rate and its resolution were limited by the memory of the oscilloscope. Nevertheless, noise clearly exhibits a Gaussian distribution.

Under the above mentioned conditions, we then estimated the CWT of the time trace of the droplet position. Figure 4.5(a) shows spectra of the CWT coefficients. The vertical scale, a time-averaged coefficient of the CWT, is dimensionless. When the noise was set at 17.8 V_{p-p}, the droplet movement shows characteristic oscillations with a period of around 2.0 sec. Essentially the same result occurs for noise with 23.7 V_{p-p}. In contrast, conditions with smaller and with larger noise levels did not induce these characteristic oscillations. There is no peak in the spectra from 0 Hz and 1.23 Hz, implying the droplet motion mainly arises from fluctuations and slow drift motion; in other words, this motion did not have typical oscillation modes. The CWT spectra indicate moderate noise amplitudes make the droplet motion oscillatory with frequency of approximately 0.5 Hz. To clarify this resonance phenomenon, we plotted the typical frequency, which is indicated by the peak in the curve [Fig. 4.5(a)]. Figure 4.5(b) shows there is a specific noise amplitude at which oscillatory motion of the droplet is induced.

4.5 Discussion

The oscillations we observed have features of coherence resonance, which was first proposed by Gang [16] in a numerical study. If a system is in a stationary state below the bifurcation point of a limit-cycle oscillation, an additive noise can induce a quasi-oscillation by exploiting the inherent nature of limit cycles. Specifically, coherent resonance extends the oscillatory region through support from additive noise. Pikovsky and Kurths found the same phenomena in the Fitz-Hugh–Nagumo system [17]. As

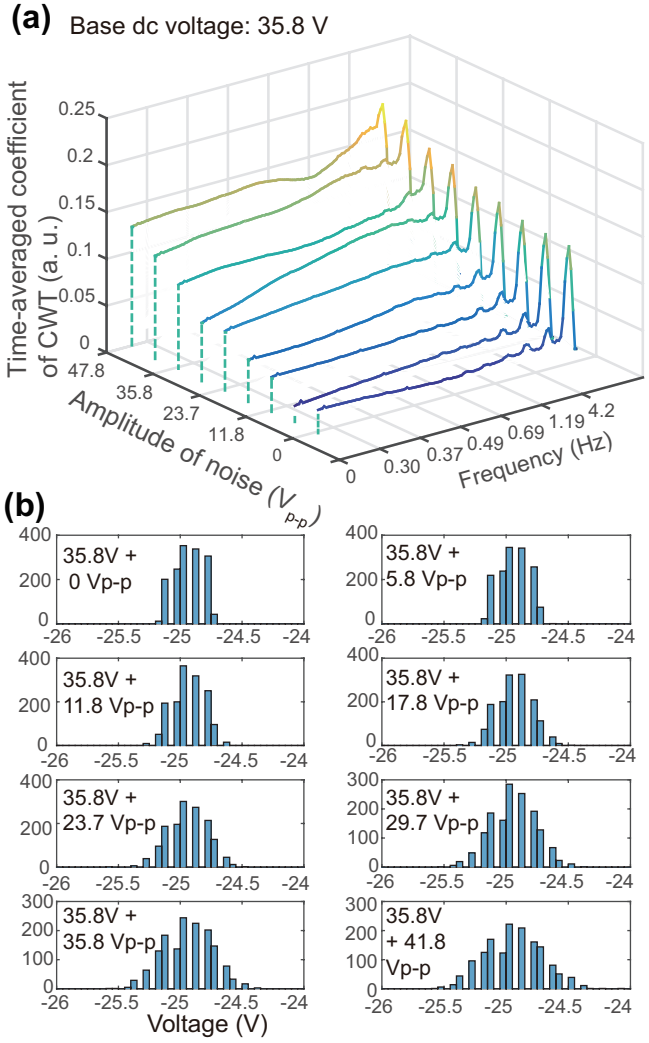

FIGURE 4.4: (a). Continuous wavelet analysis of the dc voltage accompanied with additive noise. The vertical scale, a time-averaged coefficient of CWT, represents the non-dimensional intensity. Each spectrum of the coefficient is the average of three measurements. (b). Histograms of the respective noise amplitudes based on the dc voltage. Resolution mismatching between oscilloscope and amplifier is the cause of the empty bins.

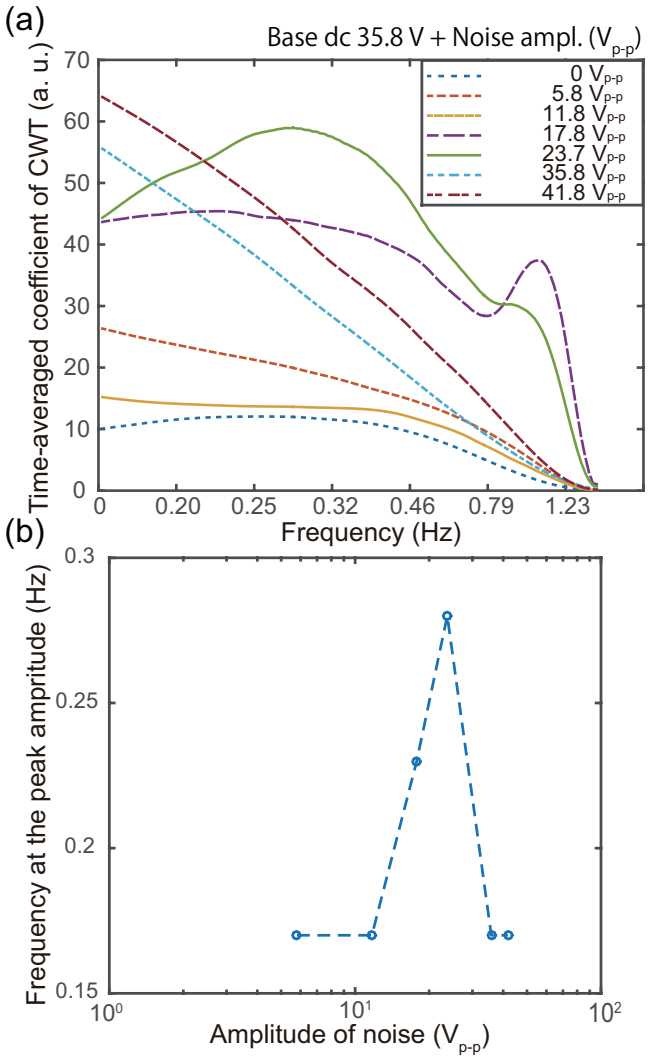

FIGURE 4.5: a) Wavelet analysis for the droplet position under various noise on the dc voltage. CWT power spectra are indicated as curves for the respective noise intensity; b) Frequency at the maximum amplitude as a function of noise amplitude.

for experimental applications, the above features can be useful in describing certain excitable systems, e.g., the Belousov–Zhabotinsky reaction [51, 52], steel pipe oscillation [53], ions through carbon nanotube channel [54], nanowire system [55], and electric circuit [56]. We have reported that the oscillatory phenomenon occurring in a droplet between the electrodes corresponds to a limit-cycle oscillation [1], which can generate excitable fixed points or weak stationary regions. In addition, adhesion of the droplet on the electrode elicits a quasi-excitable state in actual experiments. With the voltage below the threshold, and without noise, the droplet slowly fluctuates between the electrodes (Fig. 4.2) or attaches itself to the electrode and stops. Under the latter conditions, noise of moderate power dislodges the droplet from its trap. If this power is weak compared with the depth of the effective trapping potential, e.g., below 17.8 V_{p-p} in our experiments, the droplet remains positioned in the trap. However, noise with a strong amplitude, above 23.7 V_{p-p}, drives the droplet to various random degrees (Fig. 4.2). These features including the resonance behavior of noise–frequency (Fig. 4.4) exhibited in the experiments are almost the same as those of coherence resonance. The present voltage-driven actuator indicates the effective application of coherent resonance to micro- and nano-machineries

Here we note that the present noise is not truly additive but rather multiplicative. That is, the voltage noise is not external, affecting not only the electrostatic force driving the droplet but also the charge of the droplet. The terms involving noise in the governing equations complicates the solutions. We had exploited the voltage noise to use its regulatory aspect to confirm the behavioral response in experiments, but for the future, applications of light and thermal fluctuations is suggested. If this system can be down-sized to a few micrometers or smaller, then the oscillatory object is exposed to relatively stronger thermal fluctuations. A double minimum potential generated by optical tweezers has demonstrated the oscillatory motion through the use of thermal fluctuation as coherent resonance or stochastic resonance [57].

4.6 Conclusion

In conclusion, we confirmed a coherence resonance-like oscillation of a water droplet in an oil phase induced by a dc voltage applied between a pair of tapered electrodes. Certain noise amplitude on the dc bias voltage induces droplet oscillations, even below the pure dc threshold value for oscillation. In essence, the present dc voltage driven actuator can be exploited for small machinery operating under noisy environments.

4.7 Supplemental Data

All the track of the droplet of the experiment is shown in Fig. 4.6.

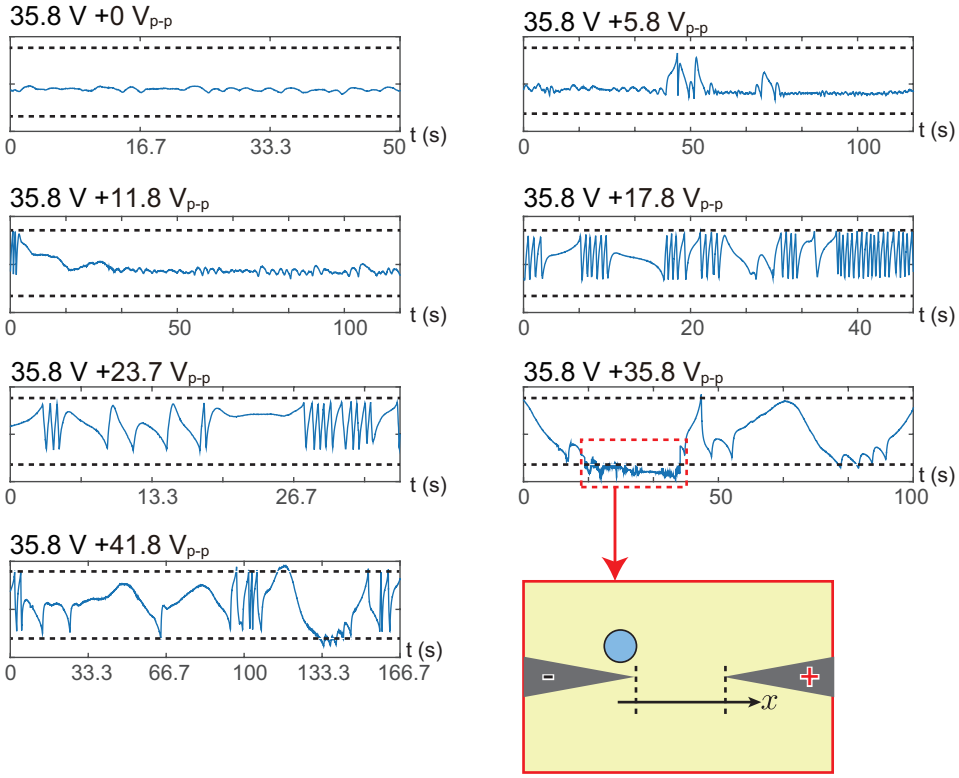

FIGURE 4.6: All the tracked data of the experiments. When $V_{p-p} = 35.8\ V$, the droplet seems to exceed the tip of the electrode. This means the droplet goes to the upper or lower side of the electrode.

4.8 Supplemental Discussion

We made the phase diagram and the numerical model of the droplet oscillation in Chapter 3. In this experiment of coherence resonance, the distance between the electrodes is smaller than 100 μm. When we do the experiment, the resonance behavior is well observed in the smaller scale. Then we think the region is corresponding to the adhesive region in the phase diagram in Fig. 3.4 and the region III in the numerical phase diagram in Fig. 3.8. The nullclines corresponding in the region III is shown in Fig. 3.9. There is two stable fixed point and one unstable fixed point. The system is a little different from the excited state. However the schematic illustration of the potential can be considered as Fig. 4.7.

Under this potential, when we add an external noise, it is expected to show a pseudo oscillation like coherence resonance.

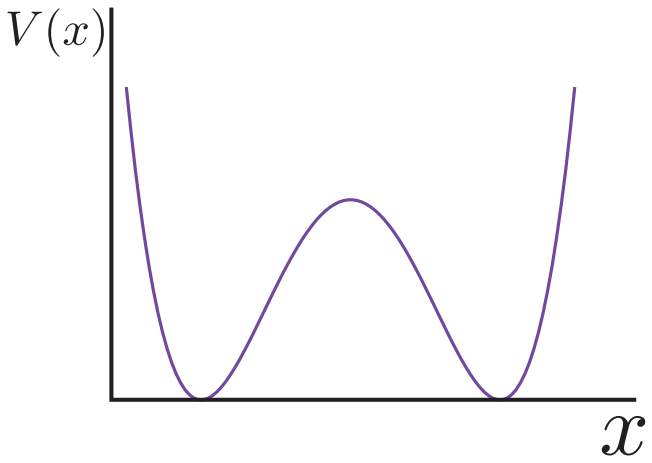

FIGURE 4.7: Schematic illustration of the supposed potential in the region III is shown in Fig. 3.9

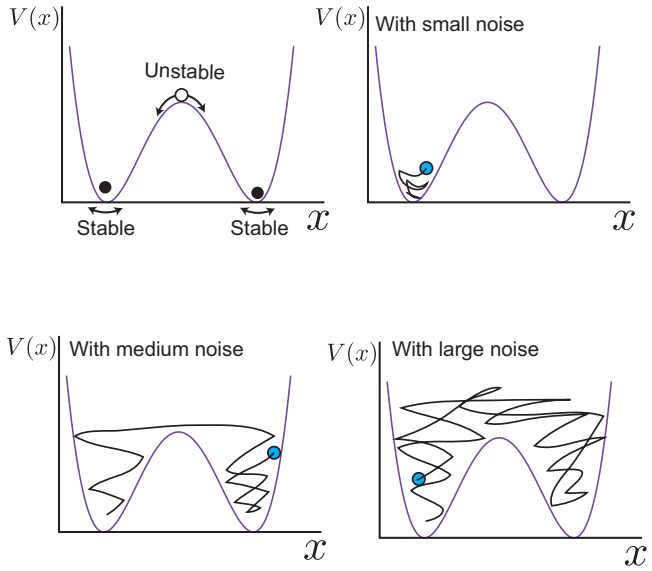

FIGURE 4.8: When the potential is like Fig. 4.7, we expected the droplet to behave as a coherence resonance. With the small noise, the droplet can not leave the fixed point. In contrast, with large noise, the noise drives the droplet randomly. With the medium magnitude of noise, the droplet can leave the fixed point occasionally and it seems to oscillate.

Chapter 5

Effect of EHD flow on micro-sized particle rotation in an oil phase

5.1 Introduction

In Chapters 3 and 4, we observed the motion of a water droplet in an oil phase. However, a water droplet easily sticks to electrodes. Droplets also coalesce easily. These features are undesirable for their application. In previous studies, it was important for the droplet to carry a charge. Therefore, in the present work, we employed plastic beads instead of a water droplet. Plastic beads cannot exhibit behavior similar to water droplets. When parallel-plate electrodes are used, the beads only line up perpendicular to the electrode [2]. On the other hand, when tapered electrodes are used, the beads revolve or rotate between the electrodes. In this chapter, we report on our discovery of the generation of regular motion of a solid plastic object under a stationary dc electric field. Interestingly, a dual-whirl rotary motion is observed for the solid object—in contrast to back-and-forth oscillatory motion observed for a water droplet—between facing sharp-pointed electrodes situated along a line. The mechanism of generation of such interesting regular motion is discussed later, along with evaluation of the effects of a coexisting surfactant in the oil phase. Interestingly, a double convective motion is generated by the application of a dc voltage. In other words, it is shown that stable rotary motion of a fluidic solution occurs and that microplastic particles undergo orbital motion driven by convective fluidic flow. We also report on the results of a numerical simulation with a simple fluid equation, indicating the reproduction of the essential aspect of the experimental trend.

5.2 Materials and Methods

A schematic illustration of the experimental setup is shown in Fig. 5.1. Polyethylene particles (Sumitomo Seika Chemicals Co., Japan) were suspended in silicone oil (KF-56, Shin-Etsu Chemical Co., Japan) containing 0.5 M surfactant; anionic surfactant, Di-(2-ethylhexyl)phosphoric acid (Sigma-Aldrich Co., USA) or cationic surfactant, Di-(2-ethylhexyl)amine (Wako Pure Chemical Industries, Ltd., Japan). We have obtained homogeneous oil phase through the mechanical agitating with a vortex mixer for 1 minute. This silicone oil containing particles was situated on a glass slide, and constant voltage was applied to the silicone oil droplet using cone-shaped tungsten electrodes. The motion of plastic particles was observed by using an optical microscope (IX71, Olympus Co., Japan).

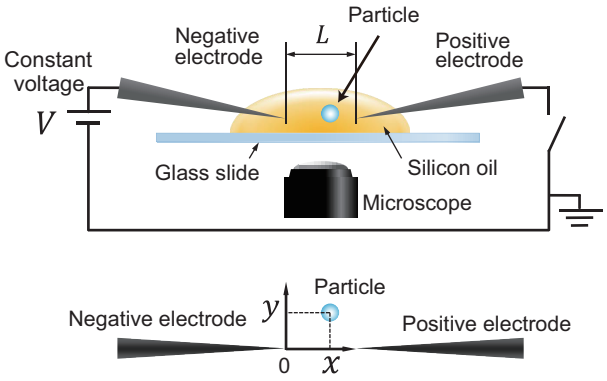

FIGURE 5.1: Schematic representation of the experimental setup. Stationary DC voltage was applied between the pair of tapered tungsten electrodes inserted into silicone oil containing polyethylene microparticles.

5.3 Results

In Fig. 5.2 is exemplified the rotary motion of number of plastic particles. It is found that dual whirls are generated on the both side with respect to the line between the pair of tapered electrodes, and that the direction of the rotations are opposite to each other. The existence of pair of the whirls suggests that the rotary motions of particles are driven under the cyclic flow of the bulk oil phase. Here, it is noted that such kind of pair of rotary motions have not been observed for the motion of droplets under constant DC voltage, where a single cyclic motion as well as back-and − force motion has been reported. Refs.

Figure 5.3 shows the angular velocity of the particle vs. the position angle during one period of the revolution. We decided the position angle as follows. When the particle is closest and farthest to positive electrode, the position angle is π and 0, respectively. The particle drives at maximum velocity when it moves from negative electrodes to a positive electrode.

Figure 5.4 shows the change of rotary speed depending on the applied voltage in the same experimental system given in Fig. 5.3. Above the threshold voltage around 60-70 V, the rotary speed increases linearly with the applied voltage. Whereas, below the threshold voltage, any motion of the particles is not generated, indicating that the transition is characterized as a kind of sub-critical bifurcation.

Figure 5.5 shows the snapshot of the particle in two different kinds of surfactants. One is the anionic surfactant(Fig. 5.5.(a)), another is cationic surfactant(Fig. 5.5.(b)). The particle shows the orbital motion of counter clockwise rotation with anionic surfactants in oil, and the orbital motion of clockwise rotation with cationic surfactants in oil. In these experiments, we have adapted the anionic and cationic surfactant with rather bulky hydrophobic group. It has been well established in colloid chemistry that such kind of surfactant with the bulky group forms inverted micelles in an oil phase, where the characteristic size is on the order of 10-100 nm being much smaller than the optical wave length. In other words, the inverted micelles with such small sizes are

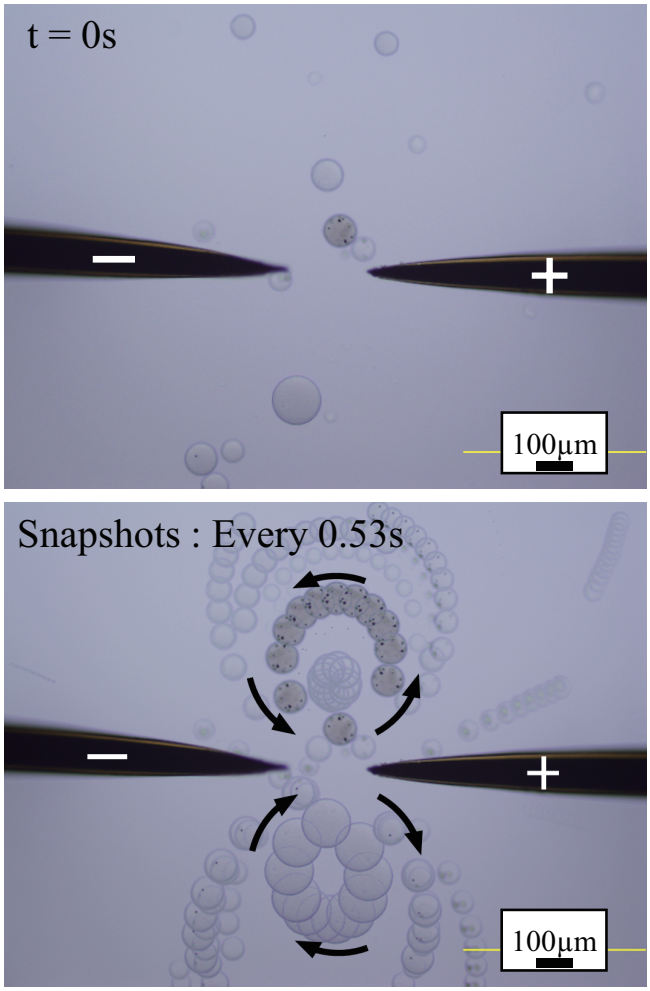

FIGURE 5.2: Self-revolution of plastic particles. (a) Initial condition at t=0 s from when DC voltage is applied. (b) Overlap of snapshots at every 0.53 s. Plural number of polystyrene particles with the radii of $r = 50 - 175\mu$m are rotating in the oil phase with anionic surfactant at V=170 V.

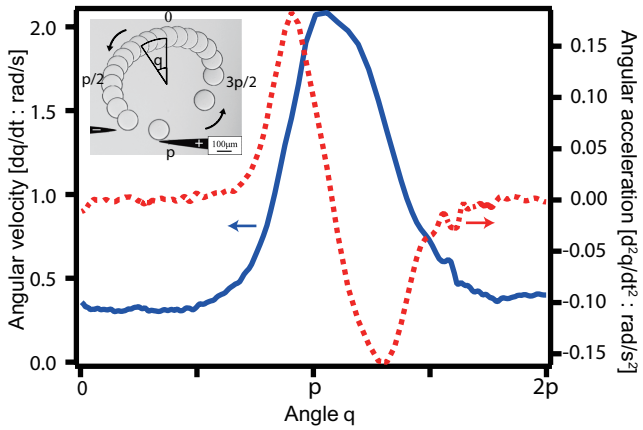

FIGURE 5.3: Angular velocity and angular acceleration depending on angular position of the particle in the presence of the anionic surfactant. The blue solid line is the velocity and the red dotted line is the acceleration. Particle size: d=175 μm. Applied voltage: V=170 V

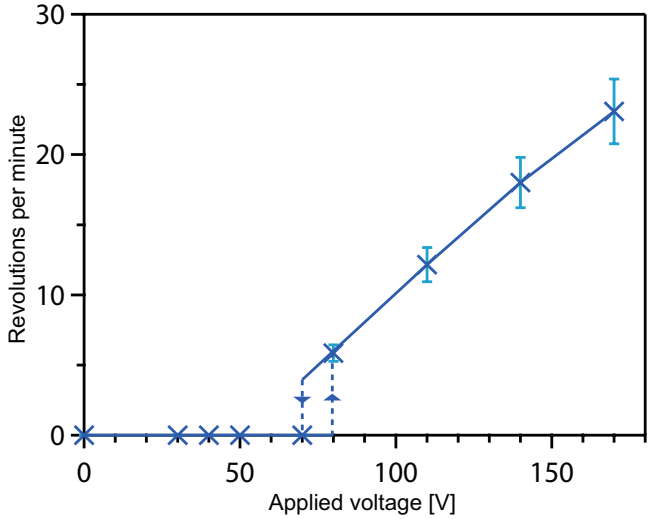

FIGURE 5.4: Revolving speed vs. applied DC voltage for a polystyrene sphere in the same experimental system as in Fig. 5.3.

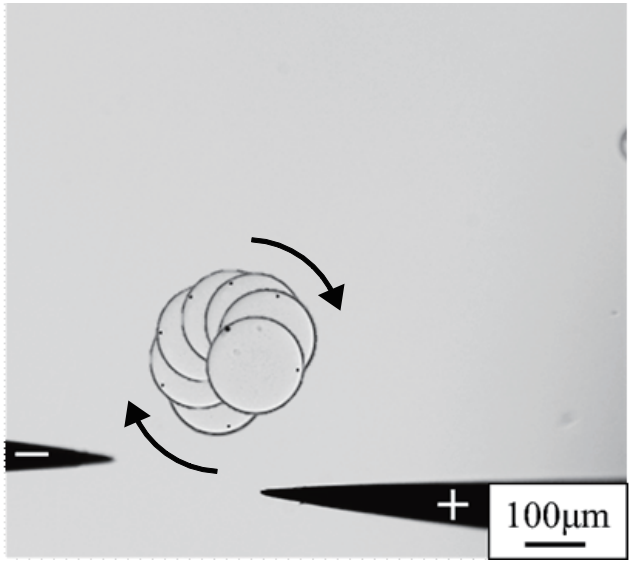

FIGURE 5.5: Overlap image on the snapshots of a polystyrene sphere in the presence of a cationic surfactant, di-(2-ethylhexyl)amine, at V=150 V, at every 0.53 s. It is noted the arrangement of the positive and negative electrodes are the same as in Fig. 5.3, whereas the direction of the rotary motion is opposite to that with the anionic surfactant.

usually transparent to optical light. The inversion of the rotary direction between anionic and cationic surfactants is, thus, attributable to the difference on the electronic acceptability. It may be reasonable to expect that anionic surfactant may gain negative charge in contact with the negative electrode, but it may be difficulty to be positively charged when it contacts with the positive electrode. The reverse situation may hold for the inverted micelles with cationic surfactant.

5.4 Numerical Modeling

The above experimental trends suggest the important role of the fluidic motion of the bulk oil phase as the plausible underlying mechanism on the twin-scroll motion of the plastic particles. In order to shed light on the plausible mechanism, we have performed numerical simulation on a simple fluidic model. We assume that invisible nano-sized inverted micelles play the role as charge carrier [58, 59]. We consider that the driving force on the micelles is proportional to the electric field. In order to abstract the essence of the mechanism, we assume that the homogeneous bulk phase containing invisible inverted micelles can carry electronic charge between the electrodes.

$$\frac{\partial \boldsymbol{u}}{\partial t} + (\boldsymbol{u} \cdot \nabla)\boldsymbol{u} = -\nabla p + \frac{1}{Re}\nabla^2 \boldsymbol{u} + \boldsymbol{E}\rho_e \tag{5.1}$$

u is the velocity of the fluid, and p is the pressure. E is the electrical field. ρ is the charge density. As the Reynolds number (Re) of our experiment is around 10^{-8}, we can neglect the inertia term from Eq. 5.1.

$$\frac{\partial \boldsymbol{u}}{\partial t} = -\nabla p + \frac{1}{Re}\nabla^2 \boldsymbol{u} + \boldsymbol{E}\rho_e \tag{5.2}$$

As for the time-dependent change of the charge density, we adapt the following equation, where ρ is the charge density at the unit volume. Here is the time-development of the charge density,

$$\frac{\partial \boldsymbol{\rho_e}}{\partial t} + \nabla(\rho_e \boldsymbol{u}) = (\sigma + \rho_e \mu)\Delta\phi \tag{5.3}$$

σ is the conductivity, μ is the permittivity of the fluid. ϕ is the electric potential, $E = -\nabla\phi$.

In the electrode configuration of the present study, near the each electrode nm-sized inverted micelles tend to be charged with the same sign of the electrical potential of the electrode. Then, we take the assumption that the medium proximal to the electrode accepts the charge from the contacting electrode.

At the first step of the numerical simulation, we calculate the electrical field. To get the electrical field, we solve the Poisson equation. The condition is as follows. The whole area we adapted for the calculation is 100×100. The positions of the electrodes are (x, y)=(0-45, 50-51) and (56-100, 50-51). The positions and shapes are shown in Fig. 5.6. The left one is a minus, and another is a plus. When we calculate the Poisson equation, we fix the potential difference as unity. We adjust the magnitude of the electric field through the coefficient that we multiply with the electrical field.

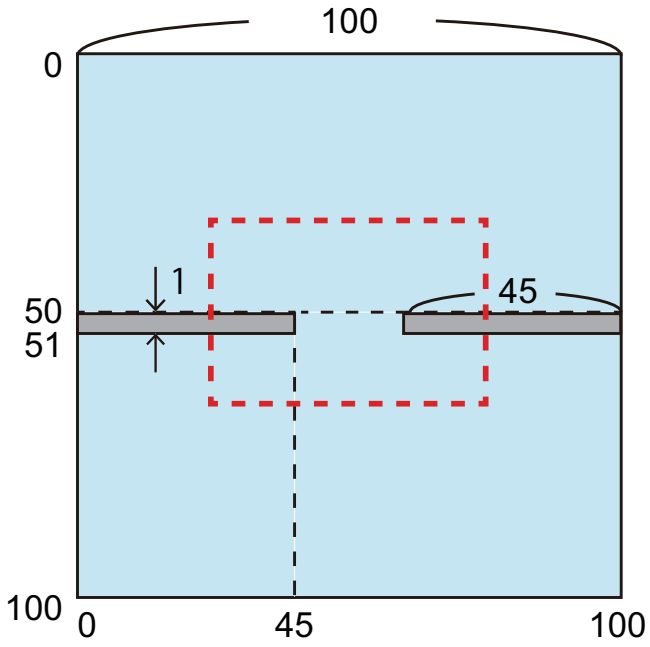

FIGURE 5.6: Geometry adapted for the numerical simulation with a pair of electrodes (gray rectangles) and fluidic region (blue). The given numbers correspond to pixel numbers. The boundary condition is taken as no-flux for simplicity. The rectangle with red dashed line is the region we showed in Fig. 5.7.

At the next step, we run the Stokes equation. We concern the periphery as a wall. The wall is far enough that does not affect the flow around the electrodes. We also consider the border of the electrode as wall. At this time, the parameters we used are Re = 0.05, $\sigma = 1.0e^{-8}$, $\mu = 1.0e^{-7}$. We fix the charge density at the electrode. That at the plus electrode is 0.5, and that at the minus electrode is -0.5.

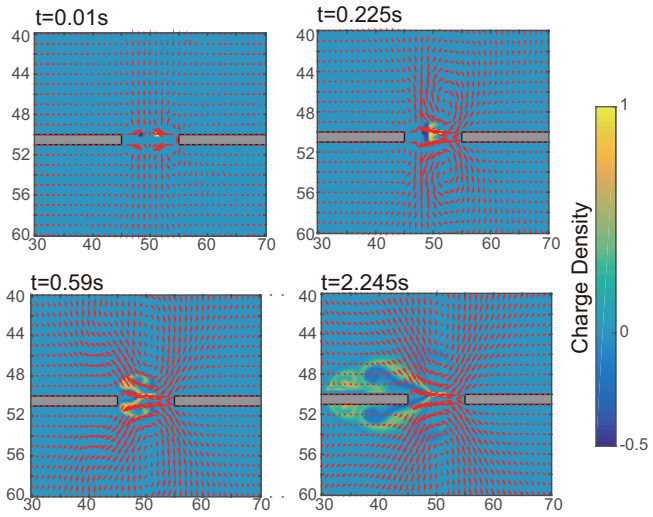

FIGURE 5.7: Numerical result on the flow profile after the application of DC voltage. The color means the charge density as in the scale given in the color bar on the right of the figure. The red arrows indicate the velocity of the liquid.

As seen in Fig. 5.7, the twin vortexes between the electrodes are generated in the numerical simulation. Where, the bulk oil solution plays the role as the charge carrier.

5.5 Discussion

In our experiment, we discover the appearance of twin scrolls on the rotary motion of the plastic beads under stationary DC voltage. In the past studies on the droplet motion, such kind of twin rotary motion has never been observed. When we use the metal particle instead of the droplet, the particle oscillates between the electrodes under DC electric field. Metal is a conductor and easy to be charged. When we use a water droplet, we can see the back-and-forth motion between the electrodes. Some groups measured how was the droplet charged. They say that they cannot consider the water droplet d as a complete insulator. On the contrary, a plastic bead is dielectric. Its dielectric constant is smaller than that of water. When we put dielectric matter under the electric field, its inductive dipole moment is along the electric field. When there are many plastic beads, the beads are gathered and linked together because of their dipole interaction. Under the uniform electric field, they stop once their dipole moment is along the field. If they are under the non-uniform field, the dielectrophoretic force along the gradient of the electric field drives them. Although without charging, the particle stops at the electrode. For this reason, we consider the fluid effect.

This phenomenon has relation to the EHD flows[60]. There are some papers describe that a dielectric liquid with some additives flows with the electrical field. They say we can apply EHD flow to a pump. With the condition of our experiment, we show EHD flow is also useful to generate a rotary motion. We can carry a micro sized thing with using this kind of flow.

Chapter 6

General Conclusion

6.1 Conclusion

In this thesis, we investigated the effects of system downsizing, noise, and flow on the oscillation of a microsized object in an oil phase. In Chapter 3, we found scale and voltage dependencies of the mode bifurcation between stationary and oscillatory states of a water droplet in an oil phase. A threshold voltage affected by the dielectric force was found to exist. When the applied voltage is under this threshold voltage, the water droplet remains between the electrodes. With a gradual increase in the voltage until it exceeds the threshold voltage, the droplet starts to oscillate. From the numerical model, we expect that the addition of noise will widen the region of droplet oscillation. In other words, noise can stabilize the oscillation when the voltage is slightly under the threshold voltage. In Chapter 4, we verified this expectation quantitatively via experiments. We added noise to the applied dc voltage and changed its magnitude. The droplet was found to oscillate well at a certain magnitude of noise with the dc bias voltage below the threshold voltage. This behavior implies that the system possesses a characteristic of coherent resonance. These results demonstrate that a water droplet oscillating in an oil phase can be stabilized by the addition of noise when the system is downsized. A microsized water droplet would be useful as a microreactor. However, water droplets easily stick to electrodes. Moreover, water droplets tend to coalesce under an electric field. In some cases, these characteristics are undesirable, for example, when we wish to use the motion of the droplet as a power source for a micromachine. To overcome this disadvantage, we employed plastic beads instead of water droplets in this work. In Chapter 5, we presented some experiments performed using plastic beads. The beads did not oscillate as a water droplet would; rather, they rotated between the electrodes. Because plastic beads are not charged, we expected them to drift along the oil flow. To confirm this phenomenon, we performed a numerical simulation. The cause of the flow was thought to be charged micelles; surfactant micelles are charged and driven by the electric field. This kind of electrically generated flow is called EHD flow. In a system with a small Reynolds number, such as the present system, laminar flow is usually dominant. However, an electric field can cause turbulence in a small-Reynolds-number system. Therefore, we can obtain an oil vortex and rotating beads in an oil phase in spite of the low Reynolds number. In conclusion, a water droplet oscillating in an oil phase is robust on the microscale. We also found that plastic beads can rotate in an oil phase by using the vortex generated by the electric field. We demonstrated this mechanism by means of a simple nonlinear physical model. We anticipate that this mechanism will be highly useful and effective in designing efficient micromachines in the future.

6.2 Future Problems

Our studies on the motion of a microsized object in an oil phase under a dc voltage have brought to the surface several problems or difficulties, and some of them remain unsolved. The following are some of the problems that need to be addressed in the future. First, in Chapter 3, we did not measure the charge of the droplet. We need to examine the process of charging during the experiment. Some research groups have measured the electric current. In our experimental system, the oil phase contains many micelles, which also carry a charge. Therefore, we cannot distinguish the charge of the droplet from that carried by the micelles. Therefore, it is desirable to visualize the charge of the droplet itself. One way to measure the charge of the droplet is to use coloring matter as a pH Indicator. Second, we found that the water droplet could not oscillate as soon as the oil containing numerous water droplets was placed on the slide. We think that this is because of the condition of the electrode surface. When we first placed the droplet-containing oil on the slide, the electrode surface was not covered by micelles. The electrodes we employed were made of tungsten, which is a hydrophilic metal. Hence, the droplets easily stick to the electrode. After a few seconds, we expect the electrode surface to be covered by micelles and to become hydrophobic. This change is important in order for a droplet to not stick to the electrode. We also expect the presence of a thin water layer around the electrode. In this case, coalescence and breaking up of the droplets under a high electric field are expected to occur, as described by Ristenpart et al. Furthermore, when we use silicone oil and a surfactant for silicone oil instead of DOPC and mineral oil, we rarely observe oscillation of the droplet in the oil phase. The droplet only coalesces with another droplet. Therefore, selection of appropriate oil and surfactant is crucial. In Chapter 4, we did not include the effects of noise in the numerical model. In our experiments, since we added noise to the dc voltage, the noise affected not only the electric field driving the droplet but also the charging of the droplet. This effect of noise is highly complicated. In Chapter 5, we found that the micelles cause flow in the oil phase. However, it is necessary to check the effects of this flow on the oscillating droplet. Apparently, no flow occurred in an oil phase containing a water droplet. One possible reason for this is that we used different surfactants in the flow experiment and the oscillation experiment. It would also be interesting to examine quantitatively whether a difference in the surfactant polarity would change the direction of rotation. In this thesis, we revealed the fundamental mechanism for driving microsized objects in an oil phase. A related issue to be addressed in the future is further downsizing to the nanoscale. All these problems are interesting from the viewpoint of not only the field of physics but also the field of chemistry and industrial application.

Appendix A

Wavelet Transformation

A.1 Introduction of wavelet transformation

In this section, we introduce wavelet transformation we used in the analysis in Chapter 4[1].

When we want to know the typical spectrum of the analog signal, we firstly use Fourier transformation Eq. A.1.

$$\hat{f}(\omega) = \int_{-\infty}^{\infty} e^{-it\omega} f(t) dt \tag{A.1}$$

Fourier transformation requires the entire time of a signal. Also, if the signal is the delta function $\delta(t - t_0)$, the Fourier transformation of the signal is $e^{-it_0\omega}$. All the component of the frequency does not become zero. In this point of view, Fourier transformation for the real signal is not suitable.

D.Gabor pointed this problem in his paper in 1964. He introduced the window function to localize the time. This Gabor transformation uses the Gauss function as the window function Eq. A.3.

$$(\mathcal{G}_b^a f)(\omega) = \int_{-\infty}^{\infty} (e^{-it\omega} f(t)) g_a(t - b) dt \tag{A.2}$$

$$g_a(t) = \frac{1}{2\sqrt{\pi\alpha}} exp(-\frac{t^2}{4\alpha}) \tag{A.3}$$

Here, $\alpha > 0$ and α is constant. In short-time Fourier transformation, we can use other suitable function as the window function. We can think Gabor transformation is the special occasion in the short-time Fourier transformation. The function suitable for the window function $w(t)$ has the character as

$$tw(t) \in L^2(\mathbb{R}). \tag{A.4}$$

The short-time Fourier transformation is written as

$$(\tilde{\mathcal{G}}_b^a f)(\omega) = \int_{-\infty}^{\infty} (e^{-it\omega} f(t)) \overline{w(t - b)} dt \tag{A.5}$$

$\bar{w}$ means the complex conjugate of w.

There is the uncertainty principle of the sort-time Fourier transformation.

$$\Delta_w \Delta_{\hat{w}} \geq \frac{1}{2} \tag{A.6}$$

[1]This section is based on the description in [61, 62].

In particular, the equation is attained if and only if

$$w(t) = ce^{iat}g_a(t-b) \tag{A.7}$$

and $c \neq 0, \alpha > 0, a, b \in \mathbb{R}$. In this thesis, we abridge the certification. But we show the schematic illustration in Fig. A.1. Gabor transformation has smaller time-frequency window in any other short-time Fourier transformation. The width and height of Gabor window are not changed as the frequency. This means Gabor transformation can not capture the too high and low frequency.

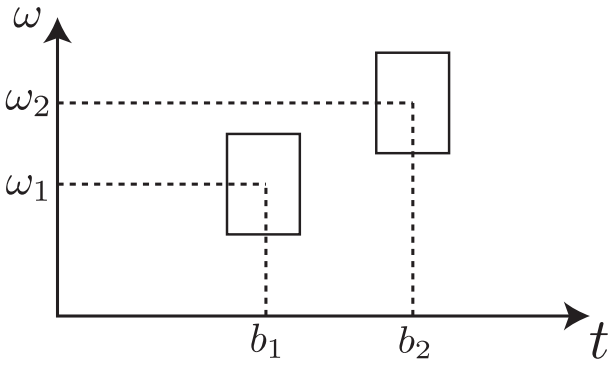

FIGURE A.1: Window for Gabor translation.

To overcome this problem, we use the wavelet transformation. In wavelet transformation, we use a mother wavelet $\psi(t)$. A mother wavelet $\psi(t)$ is like $e^{-it\omega}$ in Fourier transformation. A mother wavelet is like Fig. A.2.

We expand and translate the mother wavelet and integrate with the signal. Then we get the coefficients of wavelet transformation as

$$C(a,b;f(t),\psi(t)) = \int_{-\infty}^{\infty} f(t)\frac{1}{\sqrt{a}}\psi^*(\frac{t-b}{a})dt. \tag{A.8}$$

The mother wavelet $\psi(t)$ is scale-translated as $\psi((t-b)/a)$, then the window of wavelet transformation becomes like Fig. A.3. The width and height of those window are changed as the frequency.

There are many kind of mother wavelets. We can use them as what we want to know. Haar wavelet is one of the cardinal wavelet. Morlet wavelet, too. They are not orthogonally and compact. We can use then only for limited way. Meyer wavelet is orthognally, but is not compact. This is suitable for the signal has symmetry and infinite regularity. In this thesis, we use Symlet as the mother wavelet. Symlet is orthogonally and compact. There are similar wavelets, Daubechies and coiflets wavelets. These wavelets are suitable for the signal which has vanishing moments. They also has the character of poor regularity.

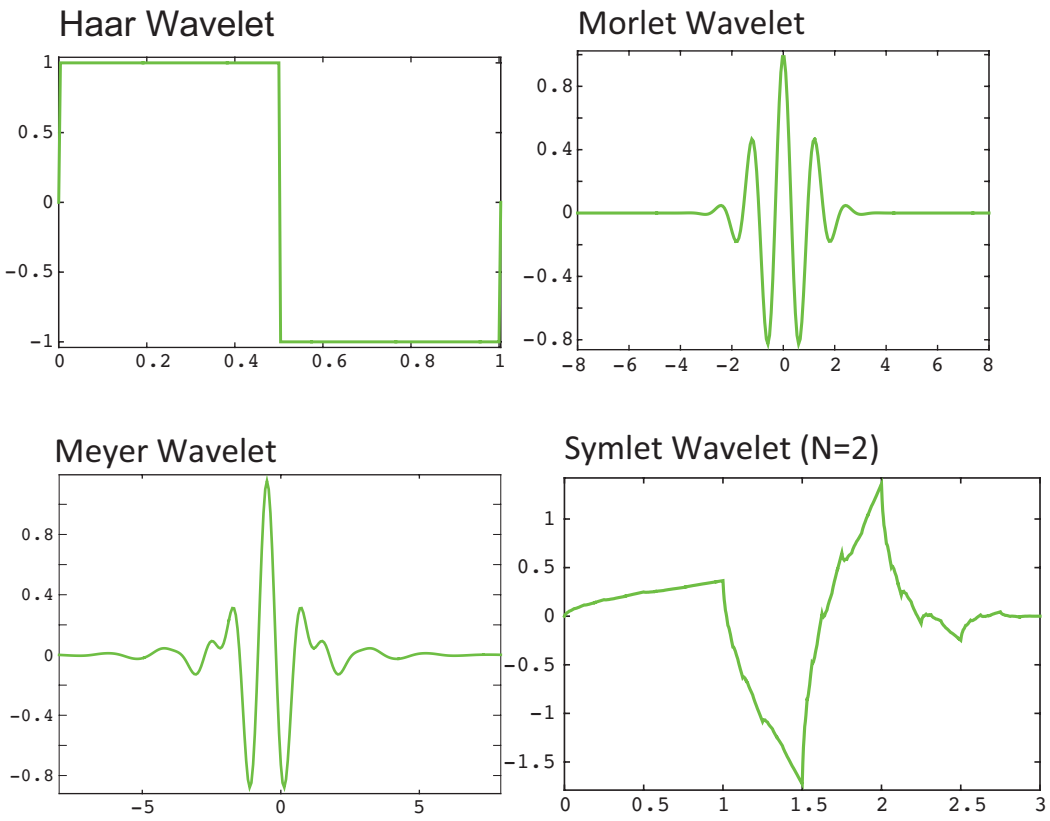

FIGURE A.2: Various mother wavelets

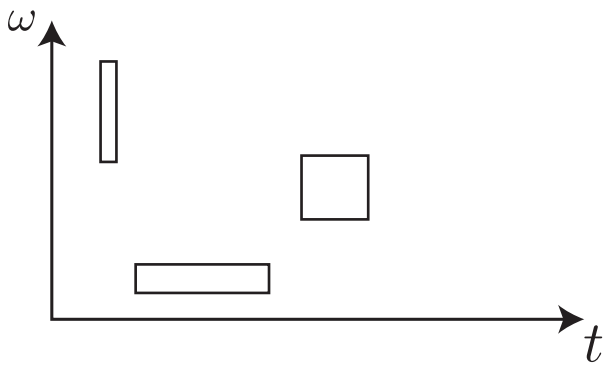

FIGURE A.3: Window for wavelet transform

A.2 Example of analysis

Here is the example of wavelet transformation Fig. A.4. To simplify the explanation, we put the sampling frequency as 1 Hz. We use Symlet (N=2) and we take the range of a as $a = 1 : 128$.

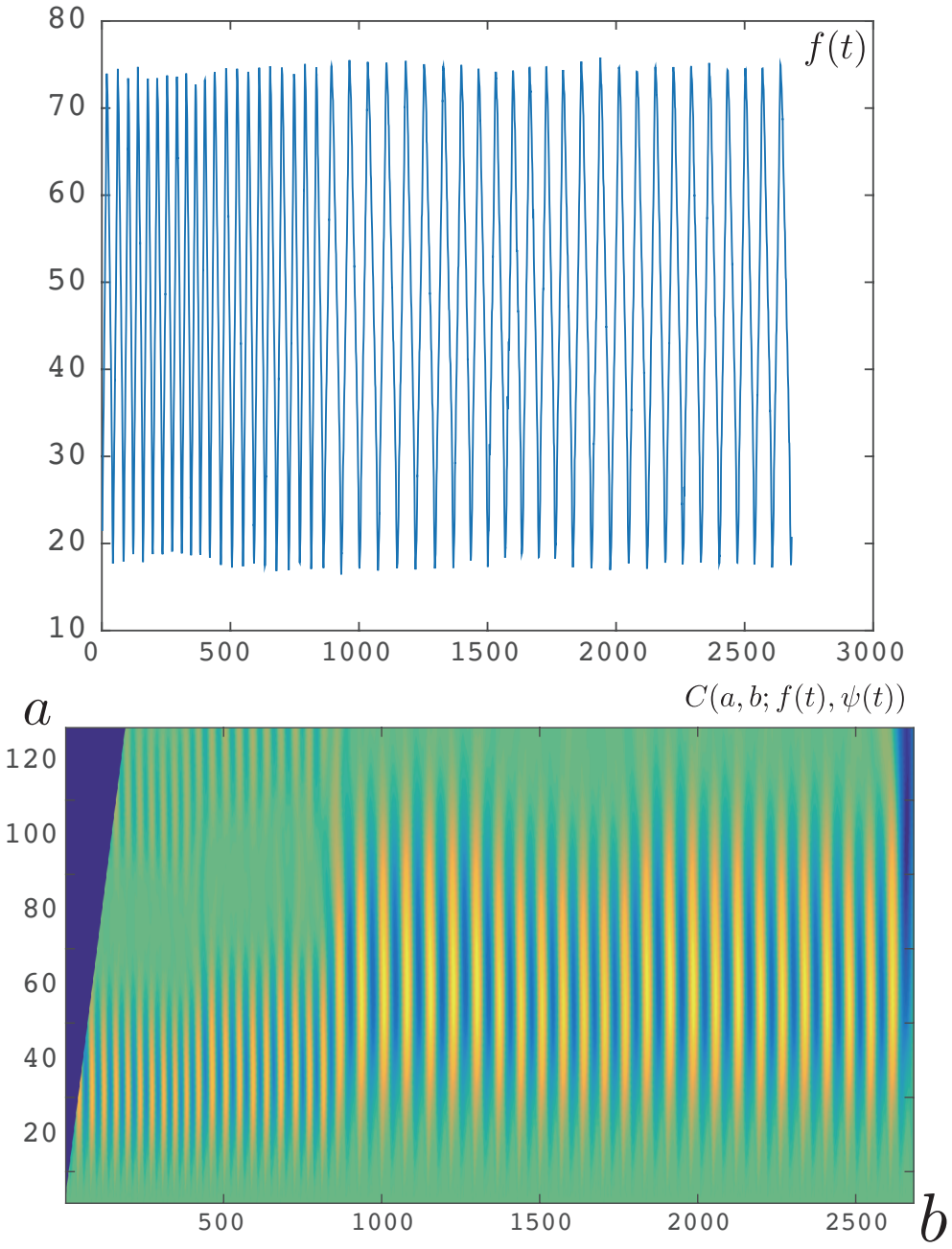

FIGURE A.4: Example of data and coefficient of wavelet transformation.

When we use other wavelets, we can get the coefficients as Fig.A.5. In this time, we think Symlet is the most suitable wavelet.

We can see the change of frequency in the signal. In $C(a, b; f(t), \psi(t))$, color means the value of coefficient, yellow is high and blue is low. There is the blue region on the right top. We can not calculate the coefficient in the region. The mother wavelet $\psi(t)$ is

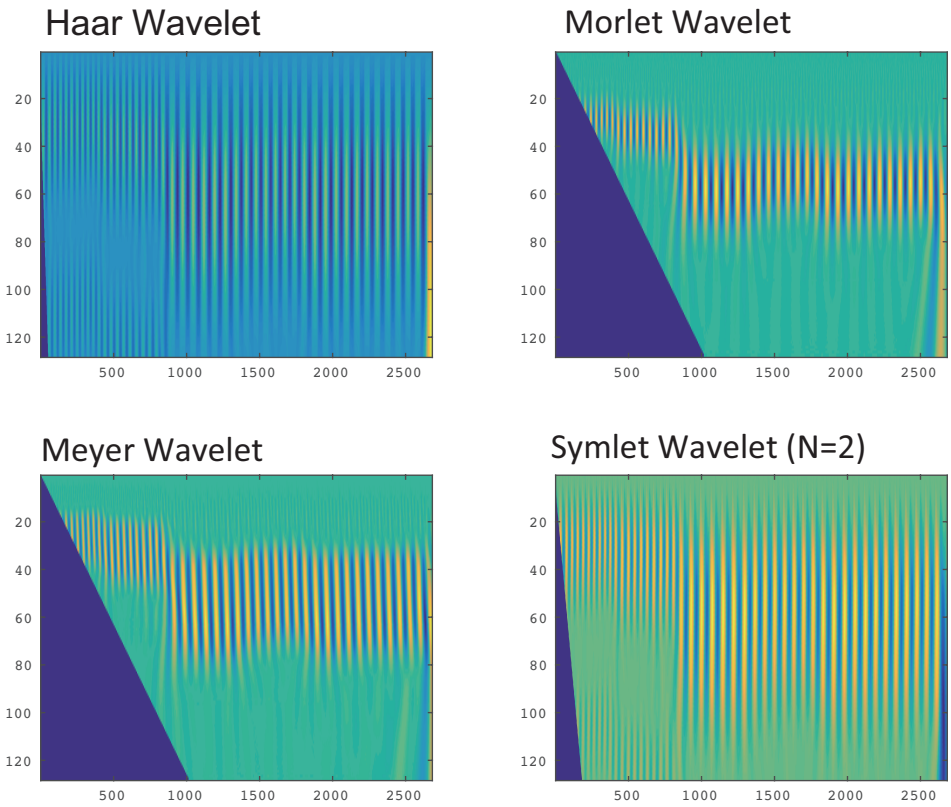

FIGURE A.5: Coefficients of wavelet transformation with various mother wavelet. We can choose a mother wavelet suitable for our analysis.

effective at $[-L, L]$. For each wavelet we use can be written as

$$\psi(t)_{a,b} = \frac{1}{\sqrt{a}}\psi(\frac{t-a}{b}). \tag{A.9}$$

This wavelet $\psi(t)_{a,b}$ is effective at $[a - bL, a + bL]$. The cone of influence is the set of all t included in the effective support of the wavelet at a given position and scale. This set is equivalent to:

$$|t - a| \leq bL. \tag{A.10}$$

We can eliminate the region by using this cone of influence. This is decided for each wavelets.

For this example, we can also calculate the cone of influence. We put the region on the coefficient map in Fig. A.6. The red lines are the limit of the valid coefficients. In the analysis in this thesis, we use this efficient area.

A.2.1 Scale to frequency

After the transformation, we have to transform the scale a to the frequency. The wavelet does not seem to have peculiar frequency. But each wavelet has the own center of frequency. Figure A.7 is the Symlet wavelet (N=2) and cosine wave of its center of frequency $F_c = 0.667$.

We can calculate the frequency F_a by using this center of frequency $F_c = 0.667$.

$$F_a = \frac{F_c}{a \cdot \Delta} \tag{A.11}$$

Here, a is the scale and Δ is the sampling period.

In Fig. A.6, we can see the time shift of the peak frequency. Now we are interested in the frequency. When $t < 1000$, we can see the scale peak is around $a = 30$. The pseudo-frequency corresponding to $F_a = 0.022$. When $t > 1600$, we can see the scale peak is around $a = 50$. The pseudo-frequency corresponding to $F_a = 0.013$.

When we use fast Fourier transformation (FFT) to the same data, we get the power vs. frequency as Fig. A.8. The results of pseudo-frequency consistent with the result of FFT. Moreover, the result of wavelet transformation distincts the frequency well.

In this thesis, we do not need the time changing of the frequency. We integrate the map along the time b and normalized (divided) by b. Then we get the scale a vs. intensity plot like Fig. A.9. we can also grasp the frequency well in this way.

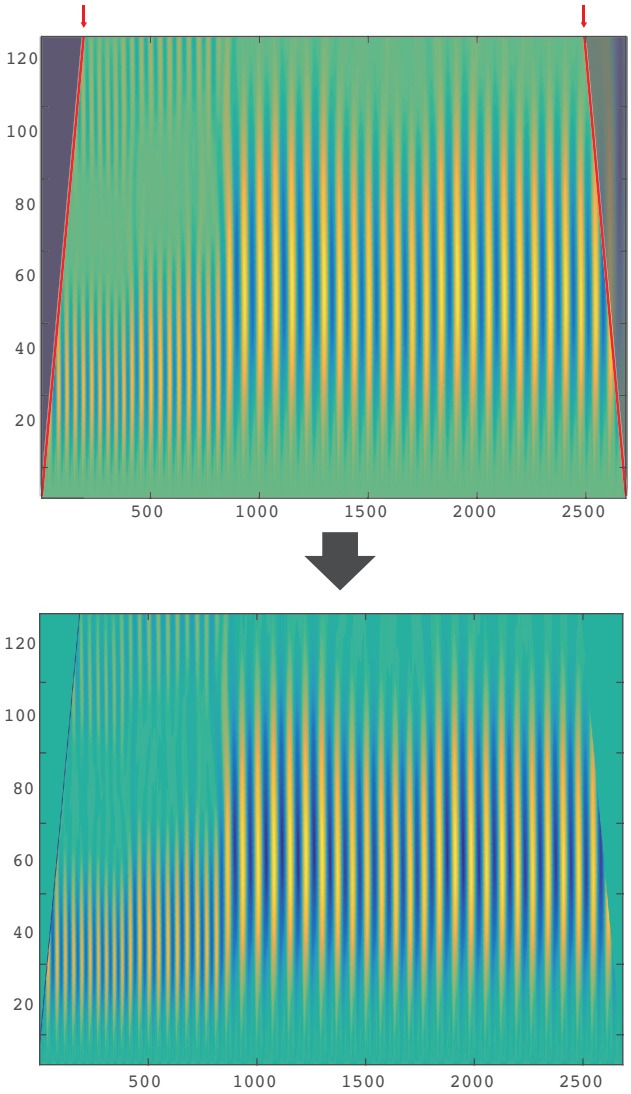

FIGURE A.6: Cone of influence is the area of the coefficients without meaningless region. The red lines show the limitation of the area. The lower map shows the coefficients eliminated the meaningless region.

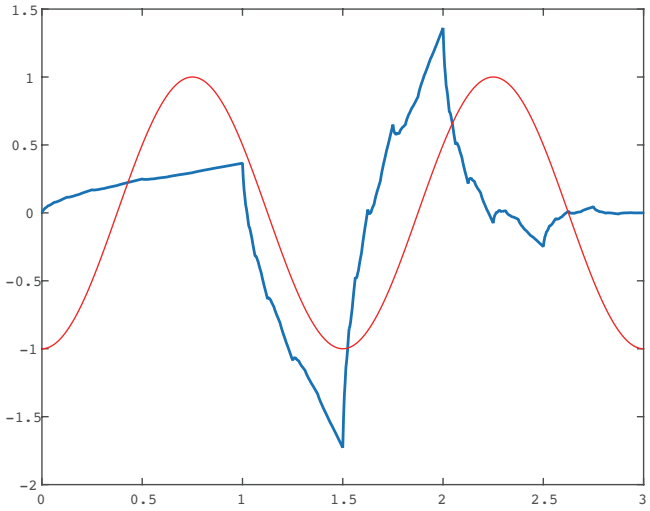

FIGURE A.7: Center frequency for Symlet (N=2).

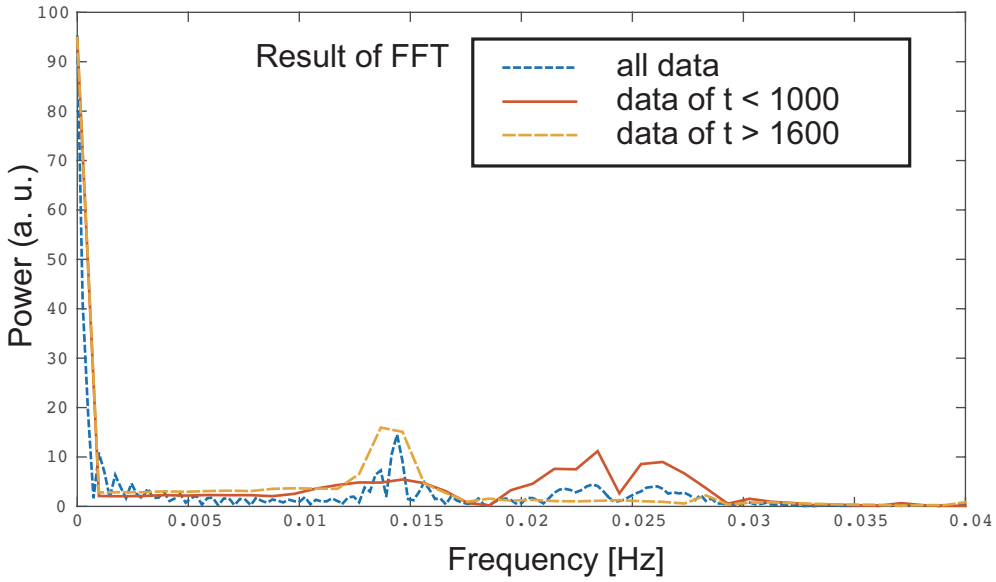

FIGURE A.8: Results of FFT with the example data, the signal of upper one in Fig. A.4. The example data has the two region of the main frequency. Blue dotted line is the results of all the example data. Red line is the results of the data $t < 1000$, which has higher frequency ~ 0.025 Hz. Yellow dashed line is the results of the data $t > 1000$, which has lower frequency ~ 0.015 Hz.

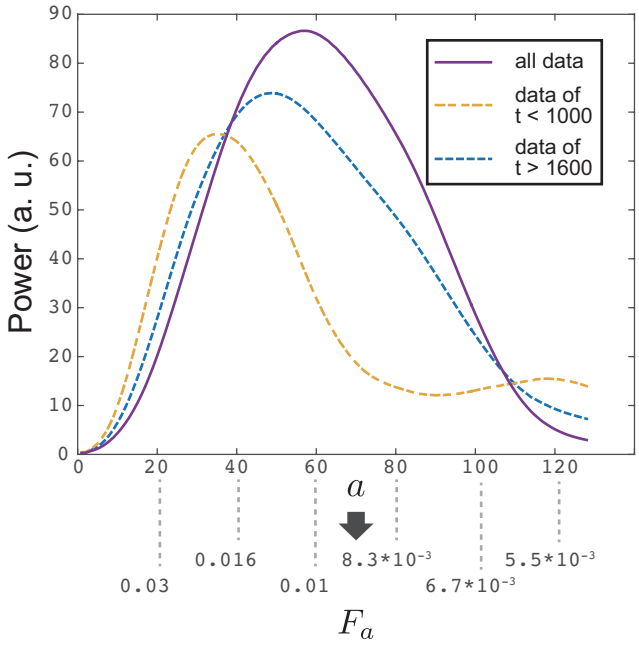

FIGURE A.9: Results of wavelet transition for the example data. The example data has the two region of the main frequency. Purple solid line is the results of all the example data. Yellow dashed is the results of the data $t < 1000$, which has the peak of the scale $a \sim 30$. This corresponds to 0.022 Hz. Blue dotted line is the results of the data $t > 1000$, which has the peak of the scale $a \sim 50$. This scale corresponds to 0.013 Hz. The result is almost the same as FFT one.

Acknowledgements

First of all, I really appreciate Dr. Masatoshi Ichikawa (Kyoto University) supporting all the things related to my research for five years in my graduate school. He helped me for writing papers, applications and so on. He has a rich knowledge and taught me many things.

I also would like to thank Professor Kenichi Yoshikawa (Doshisha University) for advising and supporting me. One reason I entered the laboratory is his style of leading student. He always encourages us. He is one of the most respectable person in my life.

I'm very grateful to Professor Masahiro Takinoue (Tokyo Institute of Technology) for teaching me many techniques of the experiments and fruitful discussion. I also thank Ms. Haruka Sugiura (Former technician of Takinoue lab.). She also told me many things about the experiment. I was very glad her about discussing and her advise about many things. I am also grateful to Mr. Masayuki Hayakawa (Tokyo Institute of Technology) for discussing. Furthermore, I'd like to thank all the members in Takinoue laboratory.

I wish to thank Professor Akihisa Shioi (Doshisha Univ.) and Dr. Daigo Yamamoto (Doshisha Univ.) for their helpful discussions. I also would like to thank Mr. Ryota Yamamoto (Doshisha Univ.), Mr. Seori Mori (Doshisha Univ.) and Ms. Masako Miki (Doshisha Univ.) for the beads experiments and their useful discussions.

I also feel grateful for Professor Yusuke T. Maeda (Kyushu University) for advising and supporting me. Especially, his advice for my English presentation was very useful. He also taught me setting the laser trapping system. I have not yet made a marked result with that, although it is a grate experience and will be useful for my future life.

I deeply appreciate Dr. Yoshiko Takenaka (AIST) for advising me and fruitful discussion. She works the research of AuNR with me now. She also supports me not only our research but also my life.

I would like to appreciate the members who were together in the laboratory: Dr. Takafumi Iwaki (Oita University), Dr. Yuko Sato (Kyoto University), Mr. Shun N. Watanabe, Professor Miho Yanagisawa (Tokyo University of Agriculture and Technology), Dr. Marcel Hörning (Kyoto University), Dr. Naofumi Shimokawa (JAIST), Dr. Yuji Higuchi (Tohoku University), Dr. Makito Miyazaki (Waseda Univeristy), Dr. Ayako Kato, Dr. Hiroyuki Ebata (Kyushu University), Ms. Seiko Hirota (Kyoto Univeristy), Dr. Akihisa Yamamoto (Kyoto University), Dr. Fumi Takabatake (Tohoku University), Mr. Daiki Kado, Mr. Eachy Liu, Ms. Yo-Ju Lee (the Vienna University of Technology), Mr. Hitoshi Hayashi (Menard), Mr. Shunsuke Tsuda (Canon) for advising and their kind help. Dr. Shio Inagaki (Kyushu University) taught me what the research is in my 3rd grade of undergraduate. I was not interested in the laboratory without the experiments and discussion with her. Dr. Takafumi Iwaki (Oita University) and Mr. Shun N. Watanabe always made me fun. Dr. Naofumi Shimokawa (JAIST) and Dr. Yuji Higuchi (Tohoku University) always looked after me. Dr. Akihisa Yamamoto (Kyoto University) and Dr. Fumi Takabatake (Tohoku University) told me many things about the research and the graduate student life.

I also would like to thank all the great OB/OGs and persons concerned of the laboratory: Professor Hideki Seto (KEK), Professor Masaharu Nagayama (Hokkaido University),Professor Satoshi Nakata (Hiroshima University), Professor Hiroyuki Kitahata (Chiba University), Professor Damien Baigl (ENS, Paris), Dr. Ayako Yamada (Curie Institute), Professor Yutaka Sumino (Tokyo University of Science), Dr. Mafumi Hishida (Tsukuba University), Dr. Ken H. Nagai (JAIST), Dr. Natsuhiko Yoshinaga (Tohoku

University), Dr. Koichiro Sadakane (Doshisha University), Dr. Akihiro Isomura (Kyoto Univeristy), for fruitful discussions in the conferences and seminars.

I appreciate the person who is a secretary for us: Mrs. Makiko Furumoto (Doshisha Univeristy), Ms. Kazuyo Fujita and Mrs. Ayumi Ishikawa (Kyoto University) for supporting my research life.

I am extremely thankful to all the current group members: Dr. Yukinori Nishigami, Mr. Hiroaki Ito, Mr. Yoshitsugu Kubo, Mr. Shunsuke Shimobayashi, Mr. Masaki Konosu, Mr. Takuya Ohmura, Mr. Kanta Eto, Mr. Hiroaki Hasegawa, Mr. Hisanori Fujiwara, Mr. Masahiro Makuta for fruitful discussion and fun days. Especially, I really appreciate my colleagues in the same grade for supporting me: Mr. Hiroaki Ito, Mr. Yoshitsugu Kubo, Mr. Shunsuke Shimobayashi. They have inspired me in so many ways.

I appreciate the supports by JSPS Reseach Fellowships for Young Scientists during PhD course (No. 27-2049), Sasakawa Scientific Research Grant (No. 24-224, 26-223) during one year, and a Research Grant from Venture Business Laboratory, Kyoto University. Furthermore, I acknowledge financial support from MEXT/JSPS KAKENHI (Grants No. 232400444, No. 25610111, No. 25610124 and No. 25103012).

In the end, I cannot thank enough my father, my mother, grandfathers, grandmothers for their supports. I am also thankful to all of my friends.

Bibliography

[1] T. Kurimura, M. Ichikawa, M. Takinoue, and K. Yoshikawa, Physical Review E - Statistical, Nonlinear, and Soft Matter Physics **88**, 1 (2013).

[2] R. Yamamoto, D. Yamamoto, A. Shioi, S. Fujii, T. Kurimura, and K. Yoshikawa, Journal of the Society of Powder Technology, Japan **51**, 823 (2014).

[3] E. M. Purcell, American Jornal of Physics **45**, 3 (1976).

[4] R Legtenberg, E Berenschot, M Elwenspoek, and J. H. Fluitman, Journal of Microelectromechanical Systems **6**, 234 (1997).

[5] E. Higurashi, O. Ohguchi, T. Tamamura, H. Ukita, and R. Sawada, J. Appl. Phys. **82**, 2773 (1997).

[6] S Kawata, H. B. Sun, T Tanaka, and K Takada, Nature **412**, 697 (2001).

[7] B. Alberts, D. Bray, J. Lewis, M. Raff, K. Roberts and J. D. Watson, "The molecular biology of the cell." (Garland, New York, 2002).

[8] S. A. Dahms and P. D. Boyer,

[9] H Noji, Science (New York, N.Y.) **282**, 1844 (1998).

[10] M. G. L. van den Heuvel and C. Dekker, Science **317**, 333 (2007).

[11] Y. Hiratsuka, M. Miyata, T. Tada, and T. Q. P. Uyeda, PNAS **103**, 13618 (2006).

[12] B. Behkam and M. Sitti, Applied Physics Letters **90**, 023902 (2007).

[13] M. Cartwbight, Journal of the London Mathematical ... **35**, 367 (1960).

[14] S. H. Strogatz, "Nonlinear dynamics and chaos." (Perseus Books Publishing, New York, 1994).

[15] J. P. Keener and J. J. Tyson, Physica D: Nonlinear Phenomena **21**, 307 (1986).

[16] H. Gang, T Ditzinger, C. Z. Ning, and H Haken, Physical Review Letters **71**, 807 (1993).

[17] A. Pikovsky and J. Kurths, Physical Review Letters **78**, 775 (1997).

[18] G. I. Taylor, Proceedings of Royal Society of London, Seies A **291**, 159 (1966).

[19] R. S Allan and S. G. Mason, Proceedings of Royal Society of London, Seies A **267**, 45 (1961).

[20] G. I. Taylor, Proceedings of Royal Society of London, Seies A **146**, 510 (1934).

[21] T. Mochizuki, Y. H. Mori, and N. Kaji, AIChE Journal **36**, 1039 (1990).

[22] J. S. Eow, M. Ghadiri, and A. Sharif, Colloids and Surfaces A: Physicochemical and Engineering Aspects **225**, 193 (2003).

[23] J. S. Eow, M. Ghadiri, and A. Sharif, Journal of Electrostatics **51-52**, 463 (2001).

[24] J. S. Eow and M. Ghadiri, Separation and Purification Technology **29**, 63 (2002).

[25] A. Khayari and A. T. Pbrez, IEEE Transactions on Dielectrics and Electrical Insulation **9** (2002).

[26] C Soria, A Ramos, and a. Perez, EuroPhysics Letters **37**, 541 (1997).

[27] M. Hase and K. Yoshikawa, The Journal of Chemical Physics **124**, 104903 (2006).

[28] D. Grier, Nature **424**, 810 (2003).

[29] D. R. Link, E. Grasland-Mongrain, A. Duri, F. Sarrazin, Z. Cheng, G. Cristobal, M. Marquez, and D. a. Weitz, Angewandte Chemie (International ed. in English) **45**, 2556 (2006).

[30] J. G. Kim, D. J. Im, Y. M. Jung, and I. S. Kang, Journal of colloid and interface science **310**, 599 (2007).

[31] Y.-M. Jung, H.-C. Oh, and I. S. Kang, Journal of colloid and interface science **322**, 617 (2008).

[32] W. D. Ristenpart, J. C. Bird, a Belmonte, F Dollar, and H. a. Stone, Nature **461**, 377 (2009).

[33] M. Takinoue, Y. Atsumi, and K. Yoshikawa, Applied Physics Letters **96**, 104105 (2010).

[34] D. J. Im, J. Noh, D. Moon, and I. S. Kang, Analytical chemistry **83**, 5168 (2011).

[35] B. S. Hamlin and W. D. Ristenpart, Physics of Fluids **24**, 012101 (2012).

[36] D. Woog Lee, D. Jin Im, and I. S. Kang, Applied Physics Letters **100**, 221602 (2012).

[37] M. M. Ahn, D. J. Im, and I. S. Kang, The Analyst **138**, 7362 (2013).

[38] D. J. Im, B. S. Yoo, M. M. Ahn, D. Moon, and I. S. Kang, Analytical chemistry **85**, 4038 (2013).

[39] S. Mhatre and R. M. Thaokar, Physics of Fluids **25**, 072105 (2013).

[40] P. Beránek, R. Flittner, V. Hroba ř , P. Ethgen, and M. P ř ibyl, AIP Advances **4**, 067103 (2014).

[41] A. M. Schoeler, D. N. Josephides, A. S. Chaurasia, S. Sajjadi, and P. Mesquida, Applied Physics Letters **104**, 074104 (2014).

[42] C. M. Phan, Journal of Physical Chemistry Letters **5**, 1463 (2014).

[43] A. M. Drews, C. a. Cartier, and K. J. M. Bishop, Langmuir, 150325153931009 (2015).

[44] a. Y. H. Cho, Journal of Applied Physics **35**, 2561 (1964).

[45] T. B. Jones, "Electromechanics of particles." (Cambridge University Press, New York, 1995).

[46] J. C. Ryu, H. J. Park, J. K. Park, and K. H. Kang, Phys. Rev. Lett. **104**, 104502 (2010).

[47] 三井 和幸, 工業教育資料, 7 (2012).

[48] S. Thutupalli, J.-B. Fleury, A. Steinberger, S. Herminghaus, and R. Seemann, Chemical communications (Cambridge, England) **49**, 1443 (2013).

[49] L. G. Leal, "Advanced transport phenomena: fluid mechanics and convective transport processes." (Cambridge University Press, 2007).

[50] K Svoboda, C. F. Schmidt, B. J. Schnapp, and S. M. Block, Nature **365**, 721 (1993).

[51] L. Zhou, X. Jia, and Q. Ouyang, Physical Review Letters **88**, 138301 (2002).

[52] K. Miyakawa and H. Isikawa, Physical Review E **66**, 046204 (2002).

[53] F. Cottone, H. Vocca, and L. Gammaitoni, Physical Review Letters **102**, 080601 (2009).

[54] C. Y. Lee, W. Choi, J.-H. Han, and M. S. Strano, Science (New York, N.Y.) **329**, 1320 (2010).

[55] P. Hessari, Y. Do, Y. C. Lai, J. Chae, C. W. Park, and G. Lee, Physical Review B - Condensed Matter and Materials Physics **89**, 46 (2014).

[56] D. E. Postnov, S. K. Han, T. G. Yim, and O. V. Sosnovtseva, Physical Review E **59**, 3791 (1999).

[57] P. Jop, A. Petrosyan, and S. Ciliberto, EPL (Europhysics Letters).

[58] F. Strubbe, A. R. M. Verschueren, L. J. M. Schlangen, F. Beunis, and K. Neyts, Journal of Colloid and Interface Science **300**, 396 (2006).

[59] J. K. Park, J. C. Ryu, W. K. Kim, and K. H. Kang, The journal of physical chemistry. B **113**, 12271 (2009).

[60] W. Kim, J. Chun Ryu, Y. Kweon Suh, and K. Hyoung Kang, Applied Physics Letters **99**, 1 (2011).

[61] C. K. Chui, "An introduction to wavelets.", 桜井明、新井勉　共訳 (Academic press, inc., Orlando, Florida, USA, 1995).

[62] 杉山博昭, 塩島壮夫, 大坪泰文, in Scej 75th annual meeting (kagoshima, 2010) (2010), p. 263.